CHAPTER 3

Depth Migration and Interpretation of the COCORP Wind River, Wyoming, Seismic Reflection Data

ABSTRACT

In order to better understand the effects of Laramide deformation, deep seismic reflection data in the Wind River (WR) Range area of Wyoming have been migrated using a 45-degree ω-finite-difference depth migration. The algorithm allows velocity to vary laterally and with depth, contains the thin lens (or shifting) term, and correctly migrates energy in laterally varying media within the limits of a 2-D algorithm and 2-D dataset. Each migrated section shown is the best from a series of migrations.

Major structural features displayed in the migrated data are the Pacific Creek (PC) anticline and the WR thrust. The PC anticline is underlain by a thrust fault similar in geometry to the WR thrust. The base of the Green River Basin sediments has a seismically observed vertical offset of 600 m. The intra-basement PC thrust reflections are as conspicuous as the WR thrust reflections, yet the movement along the PC fault was 1/50th of that of the WR fault. The reflectivity of the PC fault is attributed to the change in seismic impedance of the fault zone constituents. The thinning of sediments over the anticline in late Cretaceous time (possibly Lewis, certainly earliest Lance time) indicates that the anticline is part of the Laramide deformation. The anticline continued to grow, by faulting and buckling the lower 2 km and folding the upper sediments, during the WR thrust deformation through latest Cretaceous and Paleocene time.

The WR thrust fault is seen to ~32 km depth with an average dip of 30 degrees (assuming a N55E dip direction of the WR thrust). A vertical offset of 14 km and dip slip of 26 km is known from geologic

evidence. Although the fault zone was interpreted as planar from time sections in previous papers, it is more accurately described as composed of many strands in a wide complex zone of deformation. The fault zone increases in thickness from a zone 1 km thick at 2 km depth (known from well *and* seismic data) to at least 4 km thick at 16 km depth. The vertical offset of the fault zone decreases with depth, from 14 km at the surface, and (an interpreted) 6-8 km at 22 km depth, to a negligible amount at the base of the crust. On the migrated sections the dip segments of the fault reflection flatten at 6.6, 12, 18, 25, and 32 km depth. The reflections can be interpreted as thrust splays or as local slip zones; the reflectivity is probably due to the seismic impedance contrast of the fault zone. We explain the decrease in offset with depth and the tilting of the WR Range and Basin by curvature and flattening of the fault zone at 32 km depth, perhaps accompanied by multiple thrust splays which also decrease in dip with depth. The entire zone of compressive deformation associated with the major WR thrust is at least 50 km in lateral extent.

INTRODUCTION

Previous papers (Smithson *et al.*, 1979; Smithson *et al.*, 1978) discussed the WR data using primarily unmigrated time sections containing serious distortions due to strong lateral velocity variations. This paper presents the best of an extensive series of migrations, and the resulting interpretations. The structures revealed by migration, rather than lithologic or stratigraphic relationships, are our prime consideration.

The depth migrations of the WR data show better, more focused images of the continental crust than ever previously published. The limitation of short line length encountered at Hardeman Cty., Tx., which caused the migrated data to be severely dip-limited pictures of the continental crust (Chapter 2), is not present in the WR data. Migration moves events closer to their true position, the geometry of the structures becomes less distorted, and diffractions which obscure the

underlying signal are collapsed. Since our depth migration algorithm contains the shifting term, which is often discarded in the standard migration algorithms, energy is correctly migrated in the presence of lateral velocity variations. The more accurately imaged sections lead to new interpretations of Laramide deformation processes in the intermediate and deep crust. The ***substantial*** amounts of hydrocarbons under thrusted basement lend excitement and economic importance to the imaging and understanding of Laramide deformation.

Figure 3.1 gives the location of the dataset. Data collection has been described by Oliver ***et al.*** (1976) and Smithson ***et al.***, (1979). Briefly, this VIBROSEIS data is 24-fold, 8-msec sample rate, with a sweep frequency of 8-32 Hz. Maximum offset was 6.8 km on line 1 and 9.9 km on lines 1A and 2. The field, recording, and processing parameters are given more fully in the Appendix.

METHOD--TECHNIQUE OF MIGRATION

In this section we discuss how the migrated sections were generated. Two different migrations of the same input profile are presented in some cases because different (but valid) aspects of earth structures are emphasized by each migration. The different earth pictures result from using different velocity models: in some places the velocities are not well enough known to conclude which velocity model is more correct.

Theory

The 45-degree ω-finite-difference depth migration algorithm used to migrate the datasets shown here includes the thin lens (or shifting) term (Claerbout, 1976). Energy in laterally varying media is correctly shifted allowing for the depth-and-laterally-variable velocities within the limits of a 2-D algorithm and 2-D input dataset. This algorithm is described by Kjartansson (1979) and briefly summarized below.

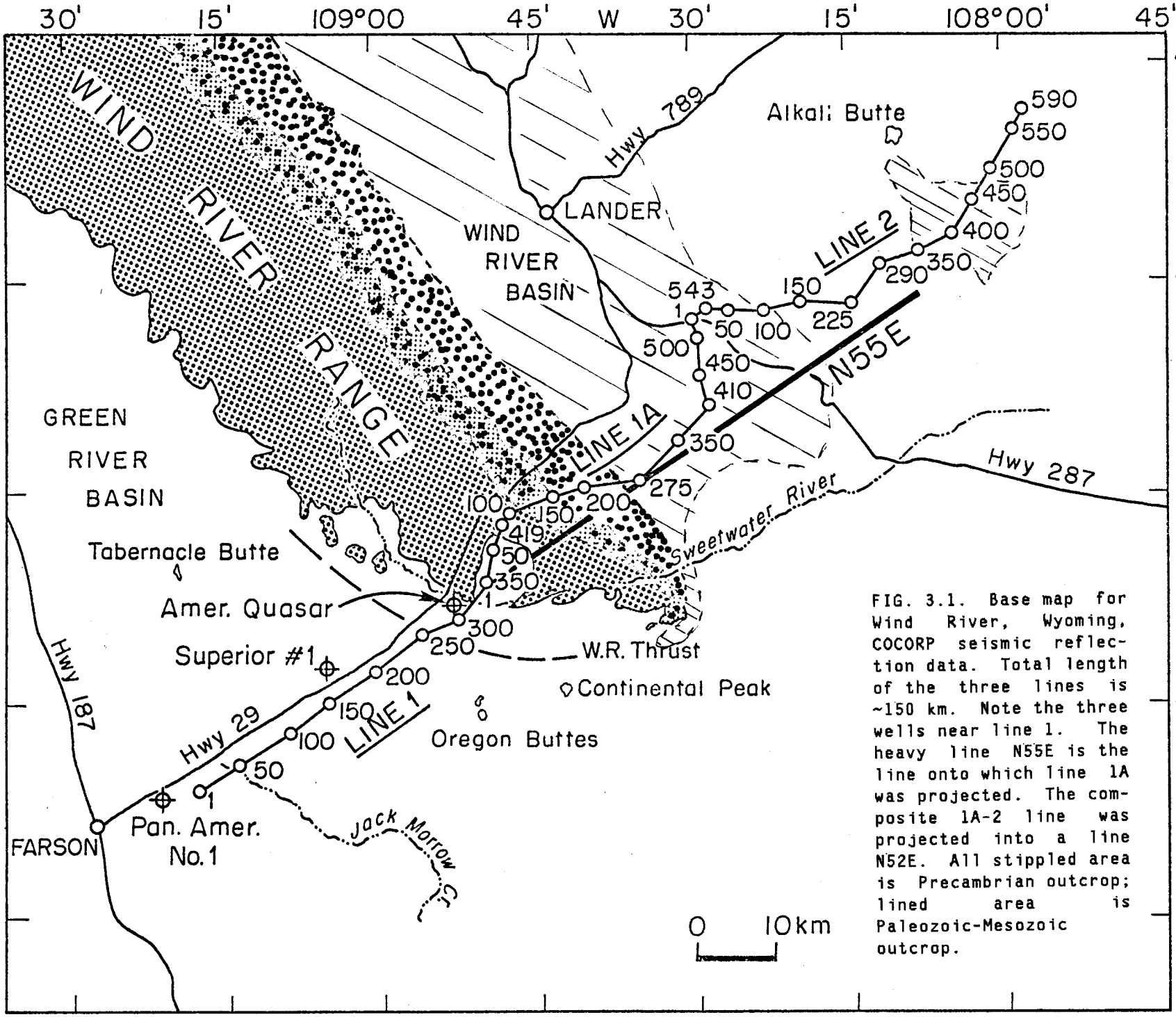

FIG. 3.1. Base map for Wind River, Wyoming, COCORP seismic reflection data. Total length of the three lines is ~150 km. Note the three wells near line 1. The heavy line N55E is the line onto which line 1A was projected. The composite 1A-2 line was projected into a line N52E. All stippled area is Precambrian outcrop; lined area is Paleozoic-Mesozoic outcrop.

The 45-degree monochromatic finite-difference program starts with an equation derived by Claerbout (1976, see Ex. 10-3-2). The two aspects of the migration operator (the diffracting term and the propagating or shifting term) may be "split" so that each part is solved separately and the results combined. The 45-degree diffracting equation which treats dipping events (or sideways motion) is

$$\frac{\partial}{\partial z} P = \frac{1}{v} \frac{v^2 \partial_{xx}}{-2i\omega + \frac{v^2 \partial_{xx}}{2i\omega}} P$$

where z = depth, P = the wavefield, v = velocity, x = the lateral direction, and ω = frequency. The time-shifting (propagating) equation also solved at each z (depth) level is

$$\frac{\partial}{\partial z} P = \frac{i\omega}{v} P$$

This approach was devised and programmed by Einar Kjartansson, with suggestions from members of the Stanford Exploration Project. The program Fourier transforms the data over time, then transposes it (into strips of x). The monochromatic 45-degree wave equation is used to extrapolate the wavefield down to the next z (depth) level one frequency at a time over a suite of (user-specified) frequencies. While all frequencies (up to the Nyquist, 64 Hz) can be migrated, we migrated only frequencies up to one-half the Nyquist. (The field filter started removing energy at 32 Hz; frequencies higher than 32 Hz were increasingly diminished.) Frequencies higher than 32 Hz (on this dataset) were often more noise than signal. Also, the fewer frequencies migrated at each z (depth) level, the quicker the run time. After the suite of frequencies is migrated, the results are summed over all frequencies at that z-level, and the wavefield at the depth z is given by inverse Fourier transforming over ω the extrapolated wavefield. Only the real part of the Fourier transform need be summed to get the migrated data at z, since the image is only the wavefield at t = 0. The output section is a depth migration.

This 2-D depth migration algorithm assumes the input to be a 2-D zero-offset section (source and receiver are co-located). Unfortunately, due to complex geology and/or a significantly crooked seismic profile, some sections of the WR dataset may be 3-D. The zero-offset section is presumed to have been generated by an exploding reflectors model, *i.e.*, waves originate from sources located on the reflectors at t = 0 and propagate toward the surface with one-half the true velocity of the medium. The common assumption, not always valid, is that this zero-offset section can be approximated by a CDP stack. The pre-stack processing must correct for "ray kinking" (irregular shot-receiver travel paths, sometimes containing short refraction paths or short pegleg multiple reflections, which result in oddly shaped "hyperbolas"). Depth migration with the thin lens term will turn the (correctly constructed) zero-offset section into a cross-section of the earth (when the dataset is 2-D and the velocity model "correct"). If on a zero-offset section the downgoing path is not the same as the upgoing path, then any post-stack migration algorithm will not correctly place that reflected energy. Full downward continuation of the field experiment can theoretically correct this problem.

The velocity model is given in z (depth) and interval velocity. The model may be constant velocity, or depth-variable (the program linearly interpolates between user-given depth-velocity pairs), or depth- and laterally-variable. When velocity varies laterally ***and*** with depth, then our particular program implements velocity gradients in z (depth) and velocity steps in x; that is, it holds the velocity laterally constant at a given depth within the lateral velocity boundaries (see Figure 3.2). When crossing from one lateral velocity region to another at a particular z-level, the velocity changes laterally with a step function. It is possible to program gradients in x (lateral extent) as well as the gradients in z, but abrupt lateral boundaries are realistic where contrasting rocks are juxtaposed by faulting (if the accurate location of the fault can be inferred). Velocity boundaries may not dip more steeply than 45 degrees without artifacts (head waves) resulting.

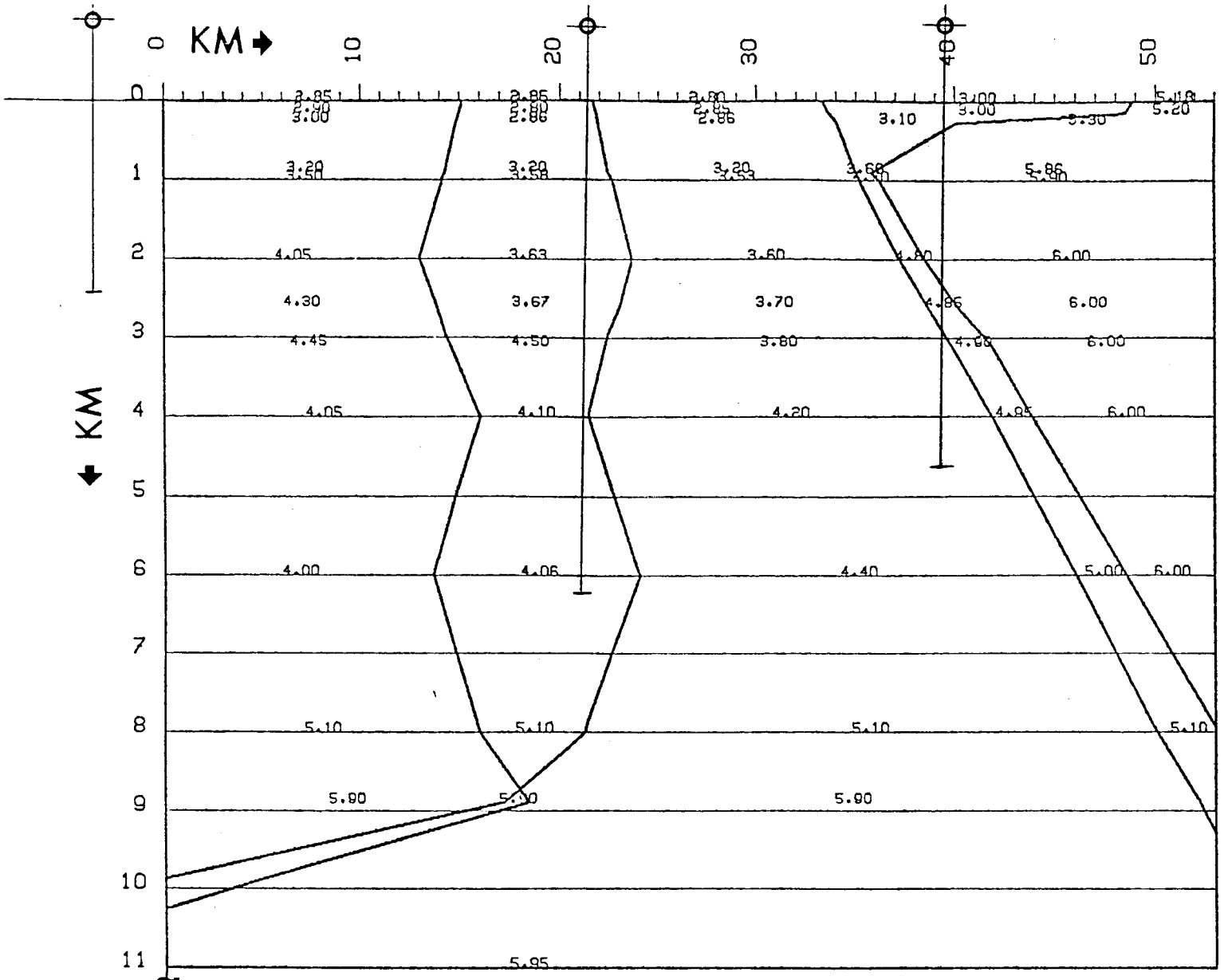

FIG. 3.2. Line 1 velocity model for migration. 4:1 V.E. Numbers in the model are interval velocities in km/s. Sedimentary velocities in the SW third of the line came from the Pan Am. No. 1 well to ~2.5 km; in the central third from the Pacific Creek Superior No. 1 well to ~7 km; in the NE third from the American Quasar well to 4.5 km. Conversion graph from km/s to ft/s.

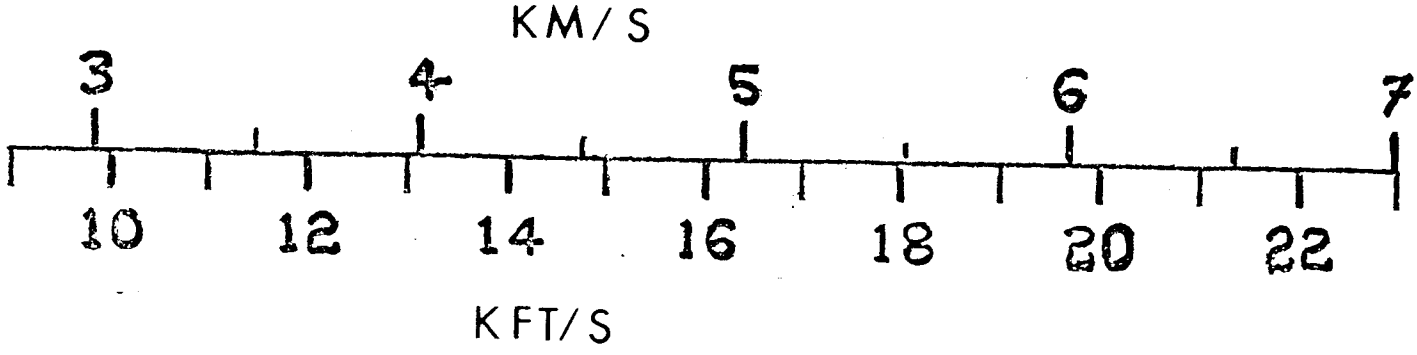

The output sections are significantly affected by the earth model used. Seismic interval velocity as a function of depth when calculated using conventional techniques (V_{rms} measured by coherence along hyperbolas and Dix's equation) is a quantity with large error bars. A large uncertainty can create error (and controversy) in the output section. We found well velocities to give better results than seismic interval velocities. On the other hand, if the velocity model comes from the interpreter's concept of structures and velocities, then obviously a significant amount of interpretation has occurred prior to migration. The ideal situation would be to use sonic log information ***and*** a sophisticated velocity estimation program that takes into account the different media seen on the downgoing and upgoing raypaths (in areas of lateral velocity variation) to estimate V_{rms} as a function of midpoint and time; the data would be stacked along non-hyperbolic trajectories; then the velocity model derived from the data would be used in the migration.

The accuracy of the depth scale is a function of velocity accuracy. We believe that the velocities used in these migrations placed shallow events (< 5 km depth) accurately in depth within 10%; intermediate events (5 to 20 km), within 15% ; deep events, within ~20%.

Line 1

Prior to migration, a post-stack adaptive deconvolution and low-pass filtering were applied at Stanford to lines 1 and 2 (Wallace, in press) to diminish the energy of multiples (Figure 3.3). A prediction distance of 1.26 sec and a prediction filter length of 0.100 sec were chosen to deconvolve lines 1 and 2, based upon the analysis of the autocorrelations. Afterwards, a 5 - 22 Hz Butterworth filter was used on the data. Peg-leg multiples in the sedimentary sequence and the longer period multiples possibly present in the crystalline crust data were attenuated. In the upper left corner (Figure 3.3, ~2.8 sec) the deconvolution operator became slightly unstable. However, low-pass filtering removed most of the problem (with respect to migration), and the migrations were not adversely affected. The migration of line 1 used the

velocity model in Figure 3.2 and is the last and best of a series of 10 migrations. The choice of migration velocities is discussed in the section entitled "Migration Velocities."

Composite 1-1A Line

In order to image the WR thrust from 0-~12 km, a composite 1-1A line (0-6 sec) was created. Stations 3-157 of line 1A were resampled using a cubic spline interpolation from a 50-m trace spacing to a 67-m trace spacing in order to mesh with line 1. Line 1 (stns. 234-350) and the above part of line 1A were composited (Figure 3.4) and migrated. The time section was not deconvolved or filtered post-stack by us. Line 1A deviates from the trend of line 1 here (see Figure 3.1): this causes some apparent seismic dips, not true dips, to be migrated. Migration of this data using two different velocity models (Figures 3.5, 3.6) produced two different earth pictures. Figure 3.5, the first velocity model, is identical to the complete line 1 and line 1A velocity models. Figure 3.6 is an alternative velocity model which used faster velocities. The velocities were not well enough known to definitively declare one model superior to the other.

Line 1A

Line 1A begins on the NE flank of the GR basin in Tertiary sediments, NE of the subcrop of the WR thrust. The line winds NE through the Precambrian core of WR Mtns., via the most accessible route. As shown in Figure 3.1, the line proceeds in 4 general directions: N15E, N80E, N45E, and N10W.

Seismic reflection data collected on such a curving profile when conventionally processed will contain apparent dips, depending upon the angle between the strike of the line and the dip of the thrust fault. Out-of-the-plane effects will also lessen data quality, and create errors on the migrated section. Our attempt to correct the crooked line problem with respect to the imaging of the WR thrust was to geometrically project the data onto a straight N55E line, and then resample the

FIG. 3.3. Deconvolved and filtered line 1, time section; 52.5 km lateral extent (shown) - 16 sec was the input to migration. Green River Basin (0-4 sec), arrow A points along the WR thrust reflection. Note time pullup of sediments under the thrust due to overlying wedge of high velocity crystalline basement (upper right corner). Arrow B points along an (interpreted) reflected refraction (along the Madison limestone). Arrow C points to Pacific Creek thrust reflection. Buried focus effect of syncline seen at location D. Base of sediments is ~4 sec. Trace spacing is .067 km.

FIG. 3.4. Composite line 1-1A, time section. 0-6 sec--31.4 km is shown, which is the input to migration. Stn. 234 line 1, through Stn. 125 line 1A shown here (basemap, Figure 1). WR thrust reflection seen here from ~0.5 to 4.3 - 4.5 sec (along arrow). Trace spacing .067 km.

FIG. 3.5. Composite line 1-1A velocity model. Numbers in the model are interval velocities in km/s.

FIG. 3.6. Alternative line 1-1A velocity model. Numbers in the model are inerval velocities in km/s.

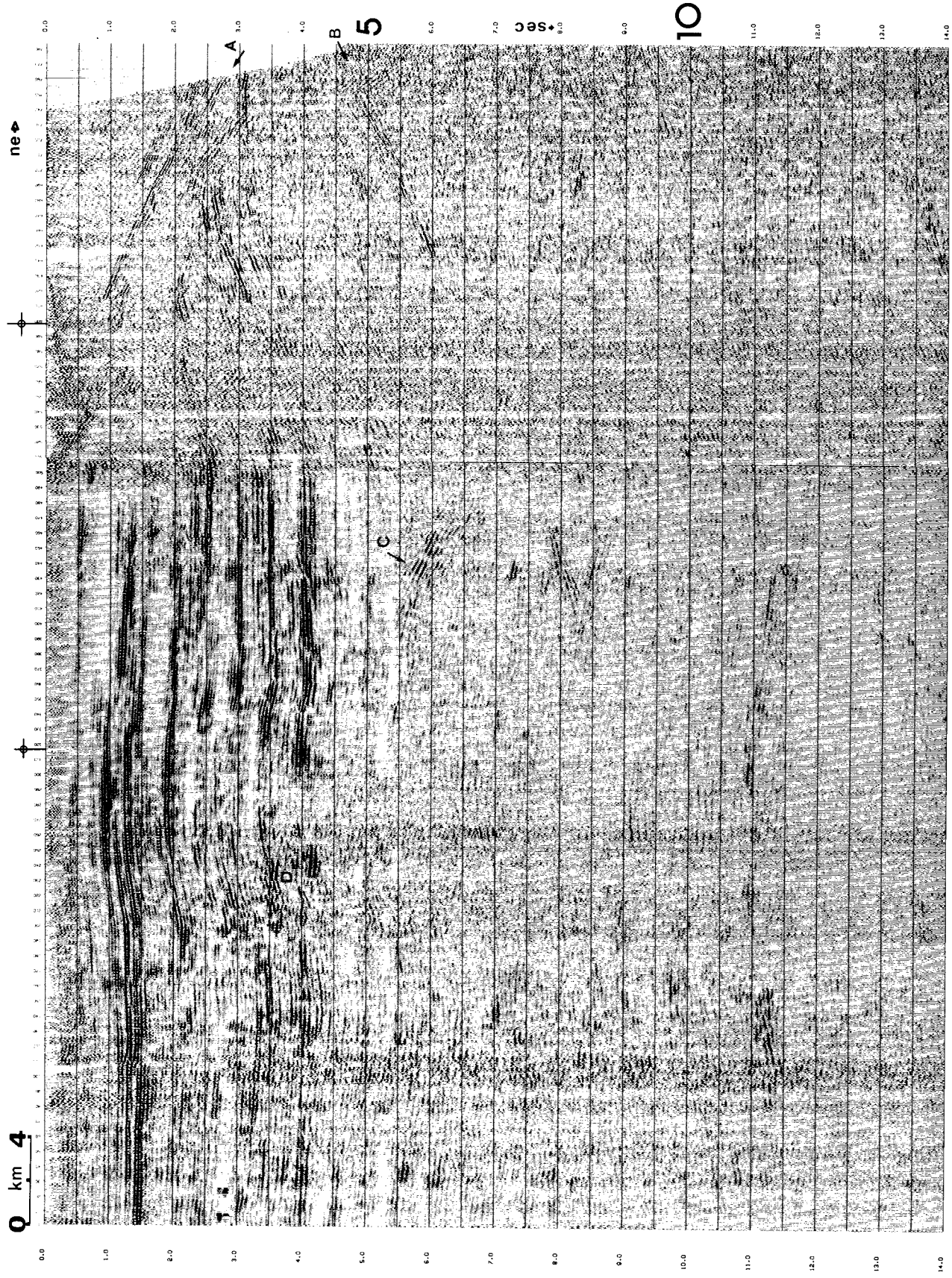

FIG. 3.3.

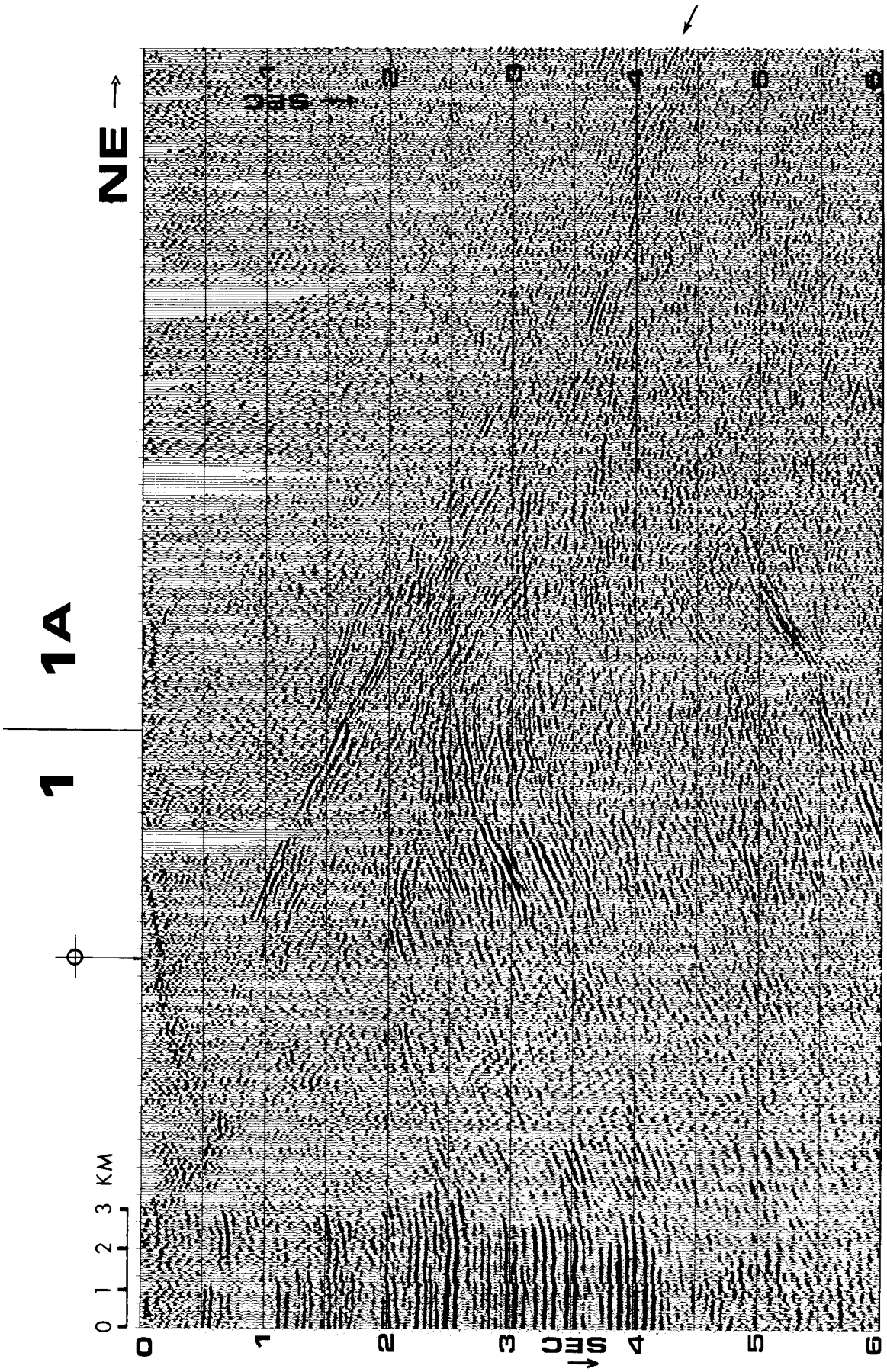

FIG. 3.4.

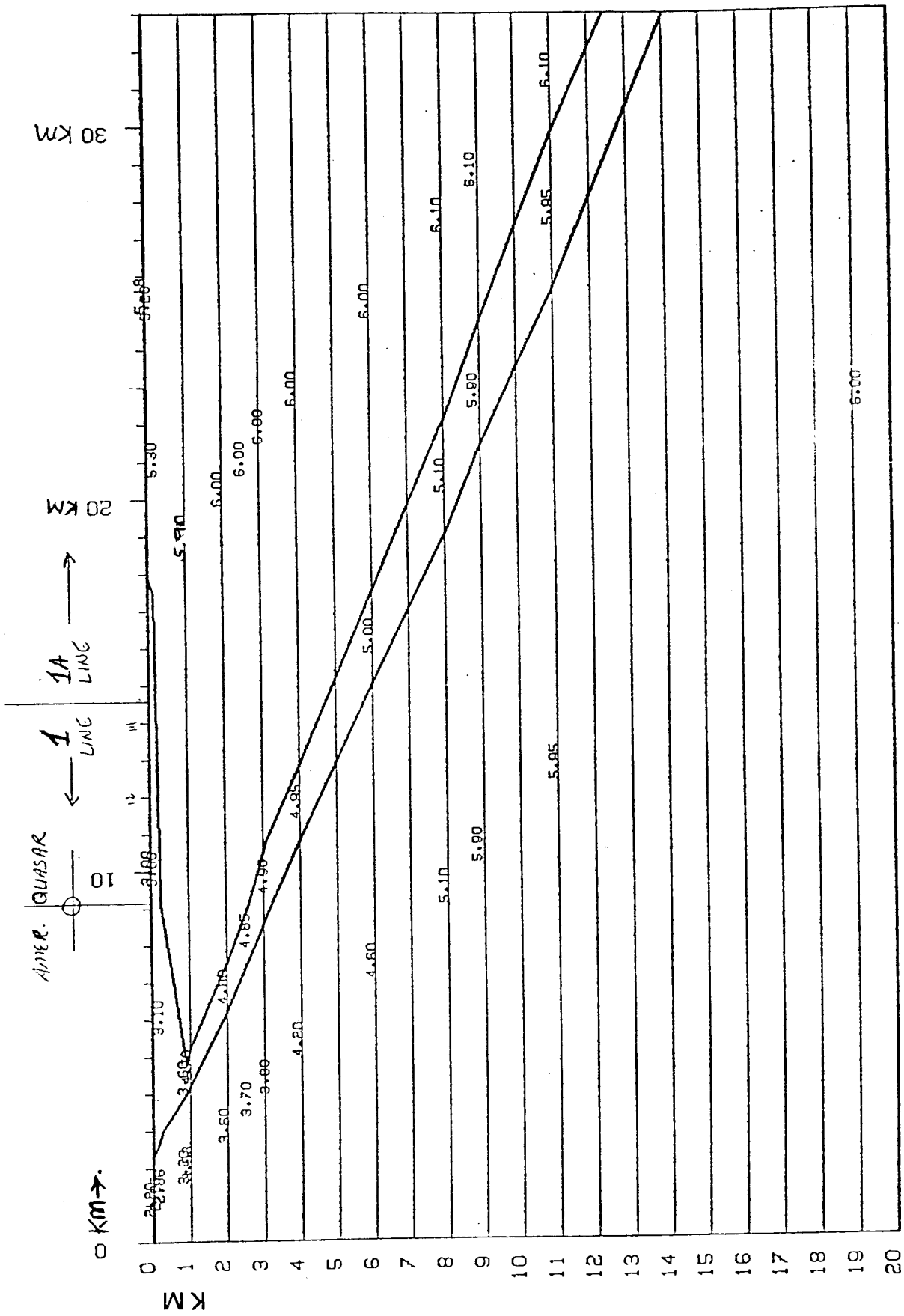
KM
0
1
2
3
4
5
6
7
8
9
10
11
12
13
14
15
16
17
18
19
20
0 KM→
10
20 KM
30 KM
QUASAR
1 LINE
1A LINE
6.00
5.90
6.10
5.95
5.30
5.10
4.95
4.85
4.60
4.20
3.70
3.60
3.10

FIG. 3.5.

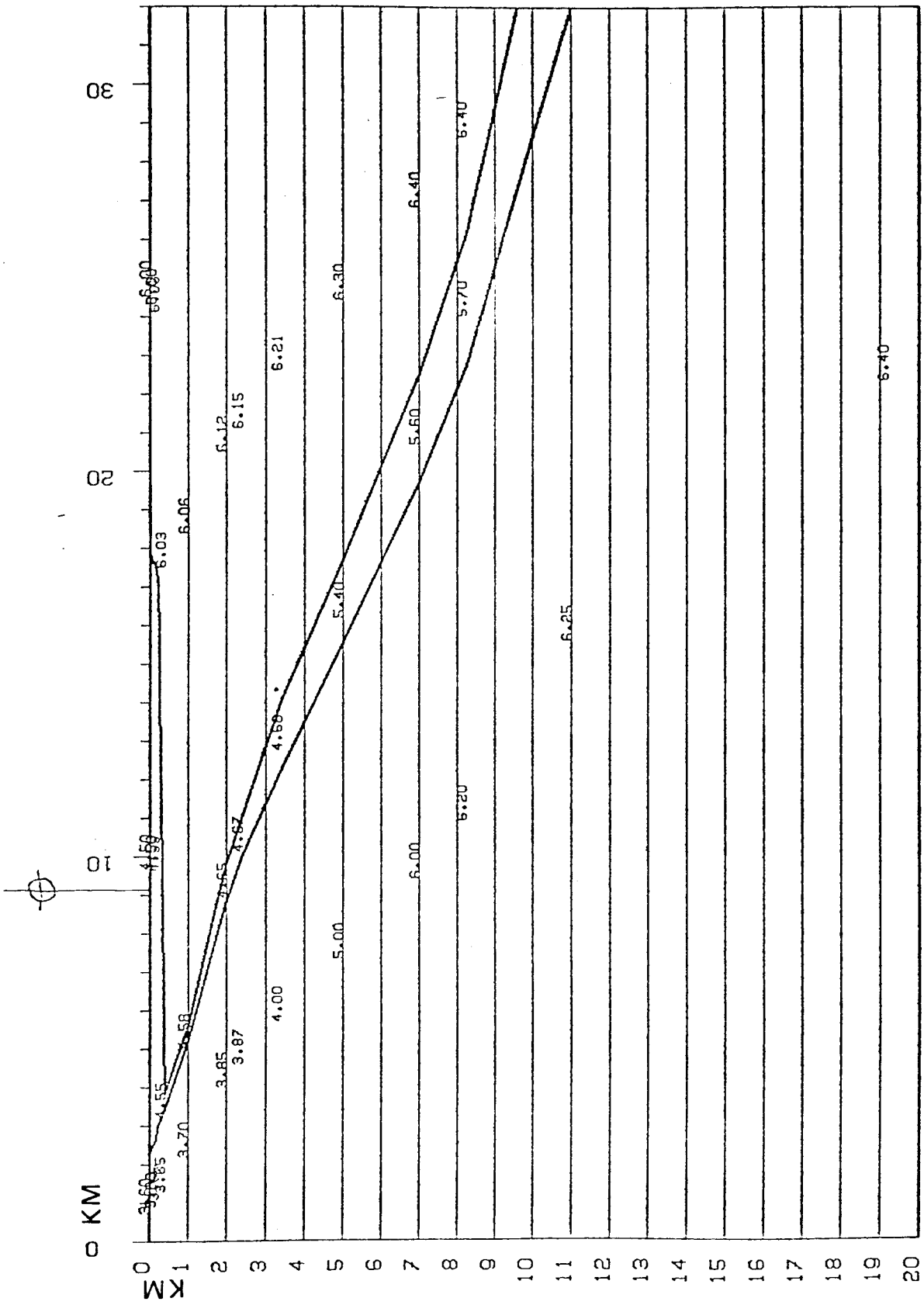
KM
0
1
2
3
4
5
6
7
8
9
10
11
12
13
14
15
16
17
18
19
20
0 KM
10
20
30
3.60
3.85
3.70
4.55
4.59
6.03
6.06
3.85
3.87
4.00
4.58
4.67
5.00
5.40
6.00
6.12
6.15
6.21
6.30
5.60
6.20
6.40
6.40
6.25
6.40

FIG. 3.6.

(now unevenly spaced) data with a cubic spline interpolation such that an evenly sampled seismic section results (Figure 3.7). N55E was chosen to approximate the mean direction of the seismic lines which is not exactly the dip direction of the WR thrust (Figure 3.1). Smithson (pers. comm.) has suggested that the dip direction of the WR fault in this area is more nearly N 20-30 E, based upon gravity modeling, which would mean that the dips observed on the migrated sections will be apparent dips, slightly less than the true dips. If features have dip directions close to N55E, the geometrical projection of the crooked line is an approximation to more accurate pre-stack processing which can correct for crooked lines. The near surface (0-3 km) at the Derby Dome (D, Figure 3.7) is obviously not 2-D. This projection technique does not remove or handle correctly 3-D energy.

The migration of the 1A line was first done by a frequency-domain algorithm (Quam, 1978), but for homogeneity within the paper (and more accuracy, since the WR basin sediments thicken to the NE), a depth migration of the "straightened" line using the velocity model in Figure 3.8 is shown here. Figure 3.8 shows our best estimate of the interval velocities; the section, "Migration Velocities", discusses this estimate further.

An "alternate" depth migration of line 1A using different velocities is included in this paper. The input time section for this migration was not straightened. The velocity model for migration was stratified and used ***seismic interval velocities*** from (average) dip-corrected stacking velocities (Figure 3.9) to migrate ~80% (traces 80-880, 9.6 sec) of the data (tic marks, top of Figure 3.7). The assumption of "stratified media" was not too badly strained by the presence of the thickening wedge of the WR basin because that part of the line was not migrated. The two differences in our "alternate" line 1A migration are: (1) a smaller, non-projected time section was the input to the migration; and (2) slower upper crustal velocities were used (6 km/s vs. 4.5 km/s). Fractured granite velocities in this region are often observed to be 4.5 km/s (pers. comm., Mark Bronston).

FIG. 3.7. Projected (straightened) line 1a, time section; 45.7 km (shown) - 16 sec was input to migration. Tic marks at top indicate the portion of data migrated with the alternate velocity model (Figure 9, Figure 22). Arrows A and B point along WR thrust; arrow C to zone of crustal reflections (~22-24 km depth). Letter D is on the Derby Dome. Trace spacing .043 km.

FIG. 3.8. Line 1A velocity model. Numbers in the model are interval velocities in km/s. Km scale on top measured from start of line 1.

FIG. 3.9. Alternate line 1A alternate velocity model. Numbers in the model are interval velocities in km/s. Compared to Figure 3.8, slower velocities to 6 km were used here.

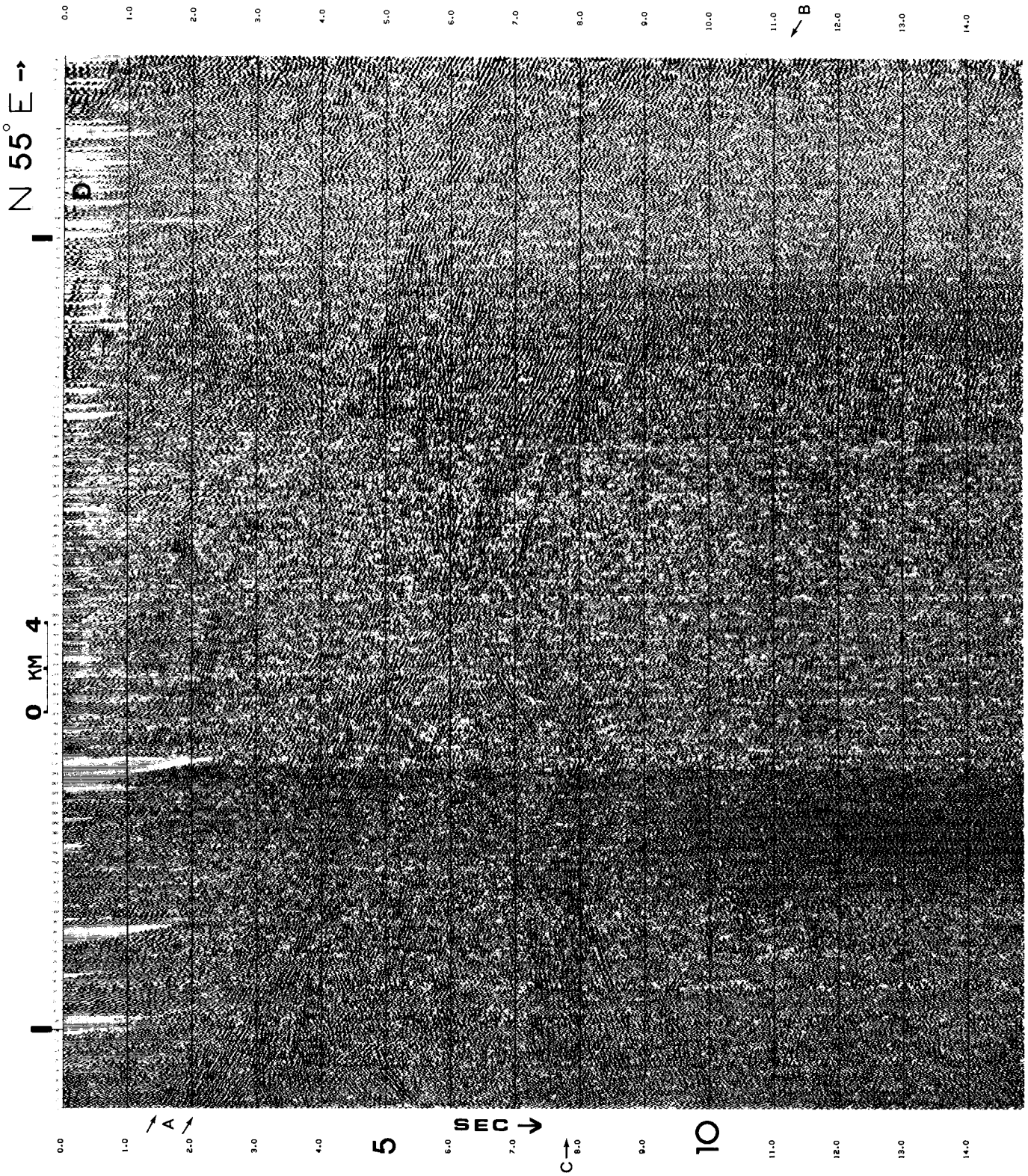

FIG. 3.7.

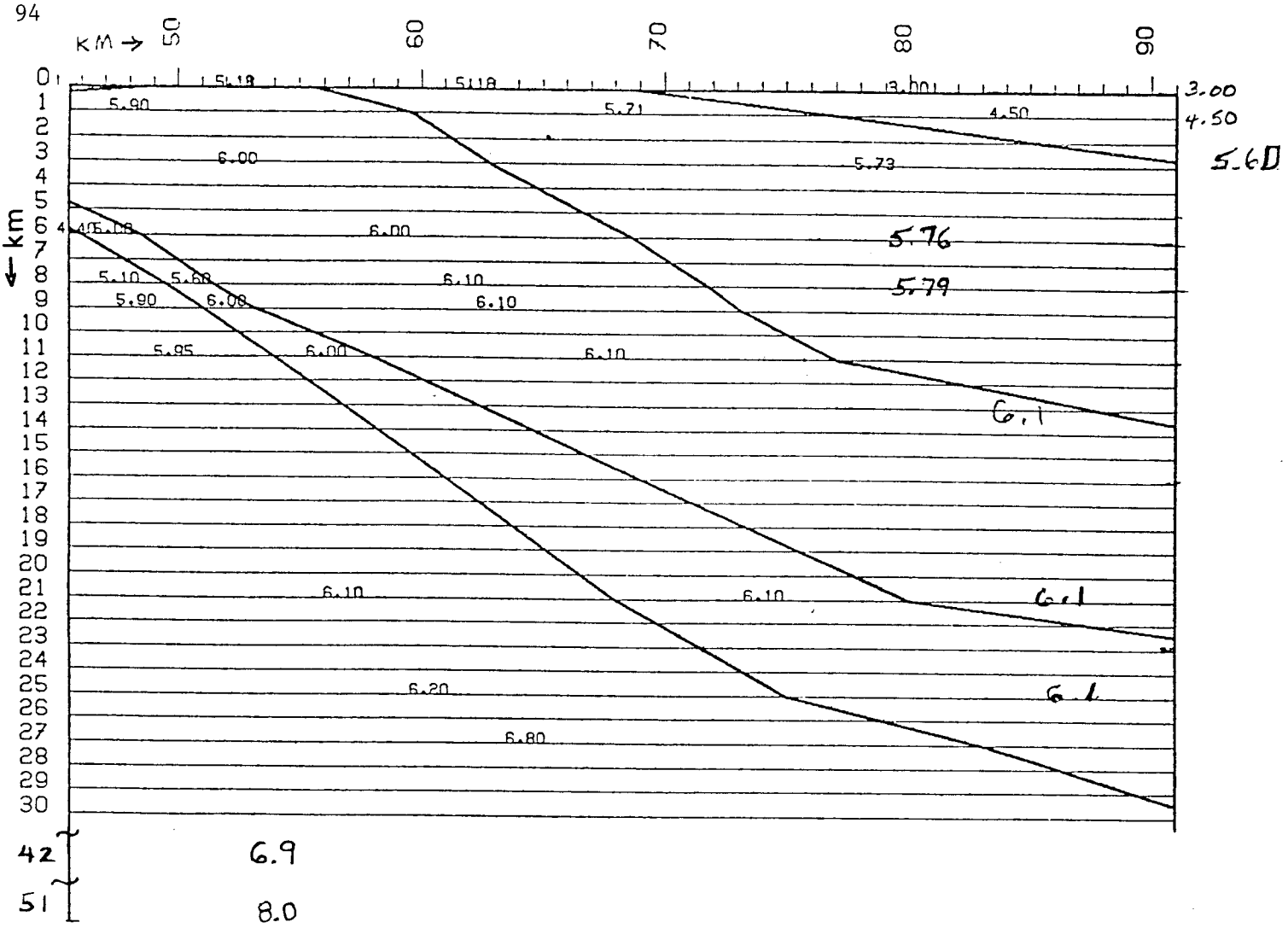
KM →
50
60
70
80
90
← km
5.90
6.00
5.10
5.90
5.68
6.08
5.95
6.00
6.10
6.10
6.10
6.10
6.10
6.20
6.80
5.71
5.73
6.10
6.10
4.50
3.00
4.50
5.60
5.76
5.79
6.1
6.1
6.1
42
51
6.9
8.0

FIG. 3.8.

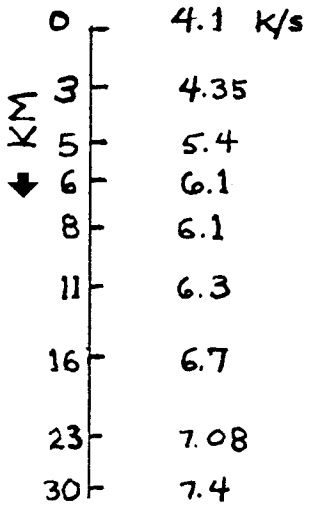
0
4.1 K/s
KM
3
4.35
5
5.4
6
6.1
8
6.1
11
6.3
16
6.7
23
7.08
30
7.4

FIG. 3.9.

Composite Line 1A-2

The last half of line 1A (stations 252.5-526.5) and the first half of line 2 (stations 15-293.5) were first composited and then projected onto a straight line trending N52E (Figure 3.10). The composition of lines 1A and 2 was necessary to portray the E-NE dips from the beginning of line 2 in their migrated location under line 1A. The part of line 2 in the composite 1A-2 line was not deconvolved or filtered post-stack at Stanford. The straightened line was then migrated using a velocity model (Figure 3.11) close to those used for lines 1A and 2.

Line 2

Prior to migration, line 2 was deconvolved and filtered (Figure 3.12) at Stanford, as discussed above. The migration of line 2 shown here is the best of 12 migrations, and used the velocity model shown in Figure 3.13. The migrations of line 1 (783 traces, 16.0 sec) and line 1A (1065 traces, 15.0 sec) used more refined computer time-sharing techniques in order to complete the long computer jobs. A migration of a 50 km by 16 sec dataset (a matrix of 1000 by 2000 points) took 9 hours on our PDP 11-70 with heavy use of an array processor. The migration of line 2 (1032 trace, 16 sec), done earlier, had to be split into three panels (with 50% overlap on the panels) to be migrated. The migrated panels were spliced to make one section.

Migration Velocities

The migration velocities are given in the velocity models (Figures 3.2, 3.5, 3.8, 3.11, and 3.13). Their corresponding migrations are Figures 3.14, 3.17, 3.21, 3.25, and 3.28. These 5 migrations are consistent with each other. The velocity model of line 1A-2 (Figure 3.11) and its migration (Figure 3.25) used slightly slower velocities to 27 km depth (to minimize upper crustal overmigration effects). Figures 3.19 and 3.22 used different velocity models; they are "alternate" migrations and do not tie with the other sections.

FIG. 3.10. Projected line 1A-2 time section; 51.5 km (shown) - 16 sec was input to migration. Stn. 1A-252.5 through Stn. 2.293.5 is shown here. To see the NE dips from the SW part of line 2 in their migrated position under line 1A, the composite 1A-2 line was projected to a straight line N52E. Arrows A point to the WR thrust, arrow B to the WR basin sediments, arrow C to the Derby Dome. Trace spacing .050 km.

FIG. 3.11. Line 1A-2 velocity model. Numbers in the model are interval velocities in km/s.

FIG. 3.12. Deconvolved and filtered line 2, time section; 51.5 km (shown) - 16 sec was input to migration. WR basic sediments are faulted at the Sand Draw anticline (location A), and again at location B. The WR thrust reflections are along arrows C. Trace spacing .050 km.

FIG. 3.13. Line 2 velocity model. Numbers in the model are interval velocities in km/s.

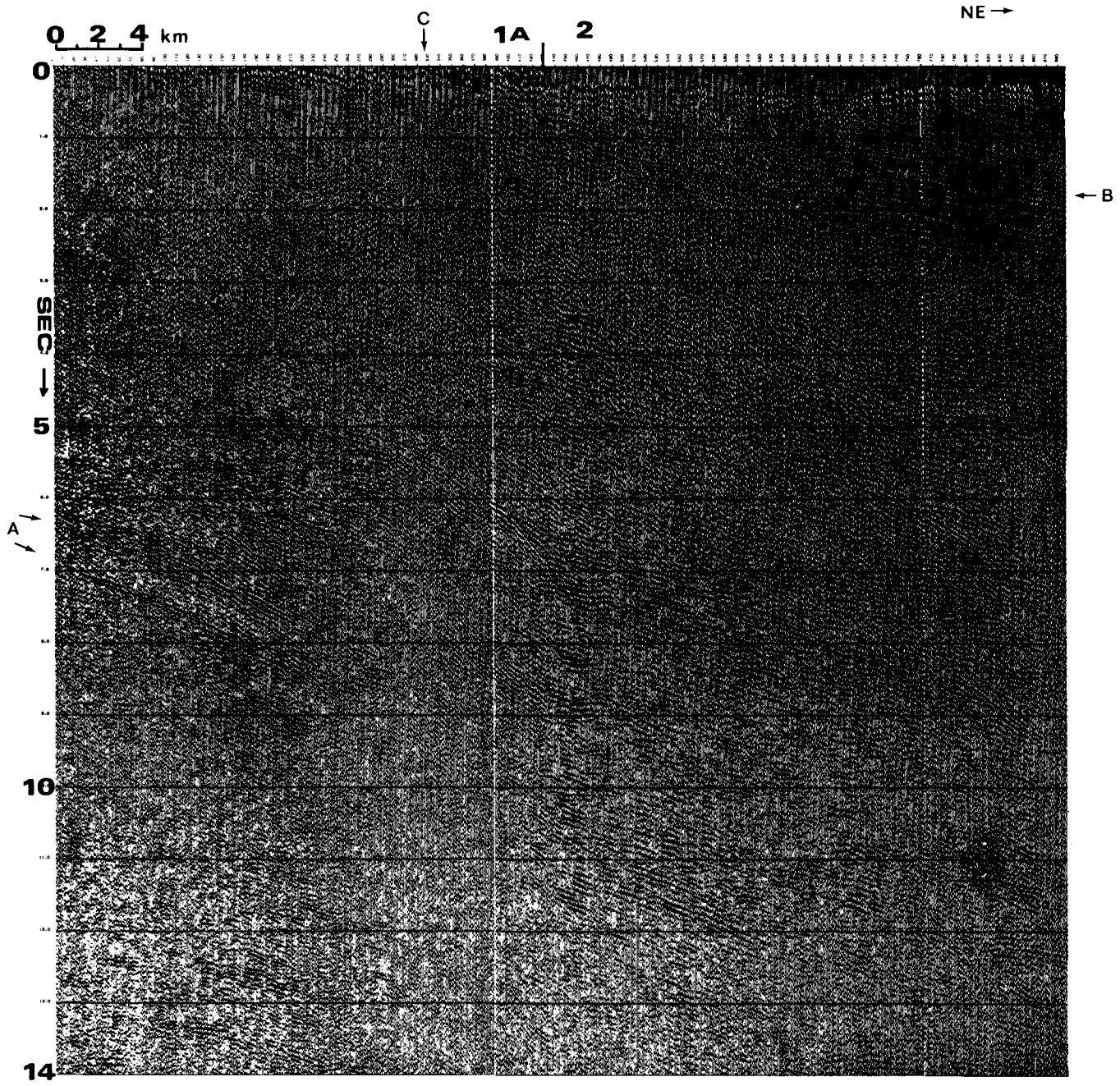

FIG. 3.10.

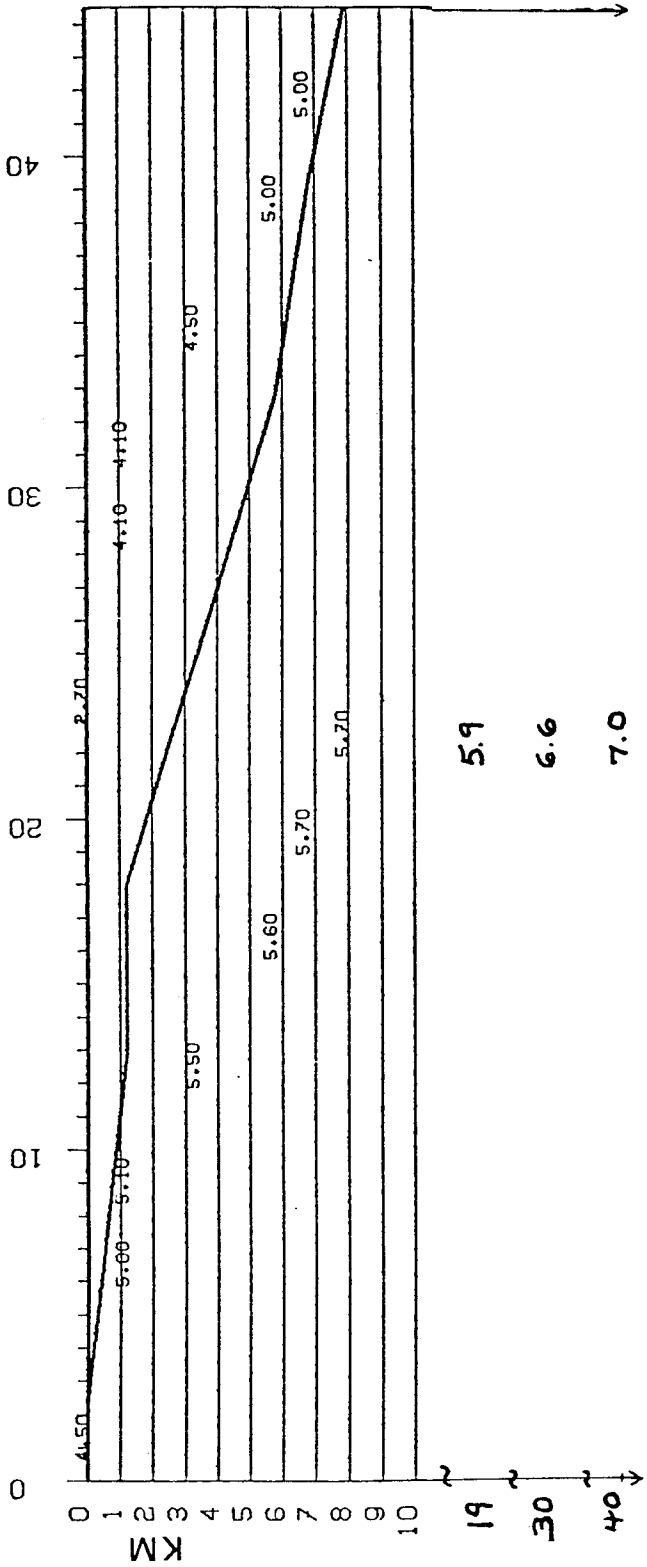
KM
0
1
2
3
4
5
6
7
8
9
10
0
10
20
30
40
4.50
5.00
5.10
5.30
5.50
5.60
5.70
5.70
5.00
4.50
4.10
4.10
2.20
5.9
6.6
7.0
19
30
40

FIG. 3.11.

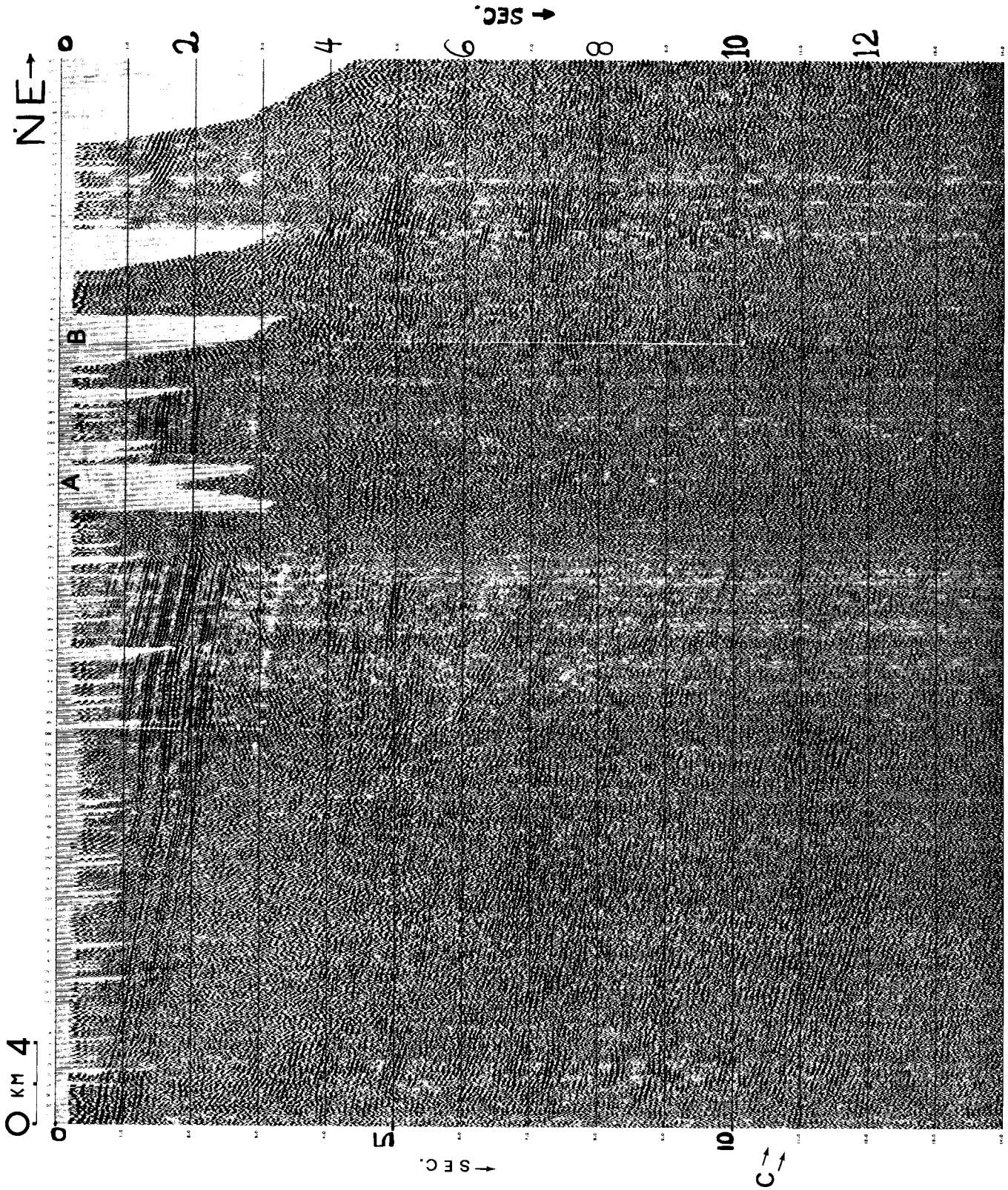

FIG. 3.12.

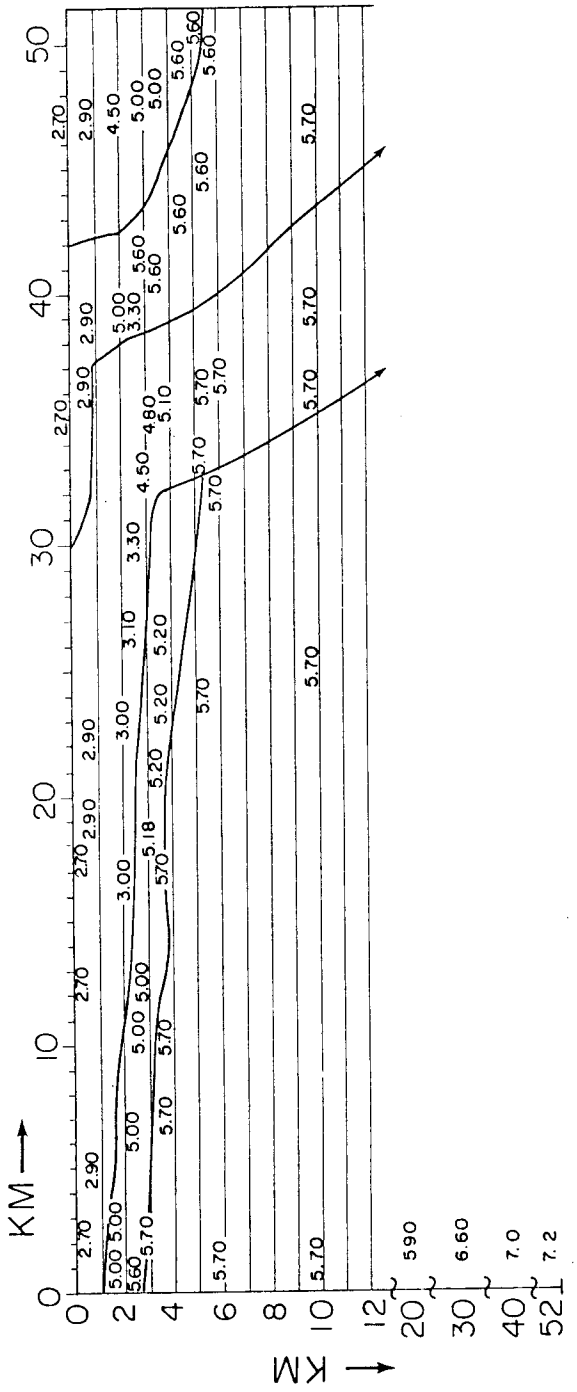
KM
0
10
20
30
40
50
2.70
2.90
5.00
5.60
5.70
3.00
3.10
3.30
4.50
4.80
5.10
5.18
5.20
5.60
KM
0
2
4
6
8
10
12
20
30
40
52
5.90
6.60
7.0
7.2

FIG. 3.13.

Shallow velocities for the migrations came directly from 3 wells on line 1 (Figure 3.2). Their location and depth is shown on the velocity models and the sections. All deeper velocities came from a borehole in crystalline rocks, 100 km to the NW in the WR Mountains (Smithson and Ebens, 1971) and from refraction work (Braile *et al.*, 1974). Laboratory data on rock type and velocity were also used to determine migration velocities.

The wedge of late Cenozoic sediments seen on lines 1-1A was assigned a velocity of 3-3.5 km/s by Smithson *et al.*, (1979). We experimented with a great range of velocities: 2.5 km/s, 3.0-3.5 km/s, 4.5 km/s, and 5.18 km/s . It was difficult to assess which of these velocities appeared to be the more correct. Therefore, Smithson *et al.'s* (1979) choice of 3.0-3.5 km/s was used.

Smithson *et al.*, (1979) reported that 7.62 km/s best stacked the WR thrust. Using a dip of 30-35 degrees, the RMS (dip-corrected) velocities are (respectively) 6.6- 6.24 km/s. These RMS velocities for the Precambrian basement are in accord with well data (Smithson and Ebens, 1971) and with regional refraction work (Braile *et al.*, 1974). However, some migration artifacts (smiles) resulted from using Precambrian velocities of 6.1 km/s. We found Precambrian velocities to ~5 km depth of 5.7-5.9 km/s produced our best migrations.

Dip Limitations

The lateral extent and the maximum recording time of a seismic profile available as input to migration govern the dips observable on the migrated profile (see Chapter 1). The typical WR migrated profile was 50 km in lateral extent and 16 sec long. Given these dimensions, the center 30 km of a migrated section can portray (will resolve) dips of either sense up to 30 degrees to 18 km depth, and up to 15 degrees to 46 km depth. *NE* dip resolution in the southwestern 20-km end of a migrated profile (*e.g.*, line 1A, line 1A-2) is excellent, though: 45-degree-dips will be observable to 30 km depth if the stack was correctly performed (see Chapter 1).

OBSERVATIONS

Line 1 Depth Migration (16 sec., ~50 km depth)

At the start (left side) of line 1, the gentle NE dip of the sediments coming down off the Moxa arch is observed (Figure 3.14). The east side of the Pacific Creek anticline (A) shows sediments folded from 0-4 km depth and faulted from 6-8 km depth (Figure 3.15). Buckling in the Paleozoic section as seen by NE dip in an otherwise southwesterly dipping sedimentary column occurs at 6.3-6.4 km (traces 220-240, Figure 3.15). NE dip is seen in all the sedimentary horizons beneath that depth to basement. From 0-6.3 km depth, the SW dip of the sediments appears to be an expression of gentle drape folding over the Pacific Creek anticline. Vertical offset of 600 m on the lowest strong reflector (Mississippian Madison limestone?) is seen. Migration turned the "bowtie" effect on the east side of the anticline at 3 sec into a syncline (traces 210-260 km, 6.6 km depth, Figure 3.15). The PC fault reflection moved updip upon migration and is most clearly seen at a depth of 11-13 km, 3 km beneath the top of the basement, with a dip of ~25 degrees (B, Figure 3.14). It can be followed (with controversy) to 16 km depth.

Interfingering of reflections within the sedimentary section indicates possible reworking of sediments (known to exist within some of the horizons), and interlayering of sands and shales. A feature resembling a carbonate platform (reef?) is seen at A, Figure 3.16, at 7.2-7.6 km depth. SW dip at 7-7.7 km (traces 460-480) in an otherwise horizontal sedimentary section, is followed by NE dip (traces 500-540). This lower section of the Green River Basin is dominantly Paleozoic carbonates.

The sedimentary reflectors underneath the WR fault on Figure 3.16 appear buckled. The easiest one to follow (4.52 km, tr. 440-510) rises to 4.25 km (tr. 545) and falls to 5.1? (5.5?) km (tr. 620). The lower horizons (6-8.8 km) are more difficult to follow, but there appear to be similar buckling and depression. A comparison of the deformation (folding, buckling) of the lower horizons in ***front*** of the Pacific Creek fault (Figure 3.15) with that of the lower horizons in front of the WR fault reveals similarities. There is some indication of overmigration in the

Green River Basin sediments west of the PC anticline and in the basement east of the PC anticline.

The deep crust shows some continuous reflectors, the strongest one being at 30 km, and some broken discontinuous reflectors (Figure 3.14). Smithson *et al.*, (1979) suggested that the mafic gneiss/schist layers exposed farther north in the WR Range could act as good reflectors but tight folding and steep dips could degrade reflections except for short segments from favorably oriented layers (p. 5963, Smithson *et al.*, 1979).

The 30 km event (at 11 sec, Figure 3.14) on line 1 is imaged best by the velocities given in Figure 3.3. Significant overmigration resulted when the following deep crust velocity function was used. Depth migrations with the thin lens term are more sensitive to velocities than the standard time migrations. Too fast velocities will dramatically overmigrate the data. Too slow velocities in laterally varying media can cause "pullups in z (depth)"; the incorrect slow velocity places energy too shallowly, thus giving the appearance of a "pullup." These migration artifacts can signify incorrect velocities or an incorrect velocity model when 2-D data are migrated. If due to raypath curvature and/or complexity, certain geologic horizons are not recorded, but "should be" on the sections, then migration artifacts due to truncated reflecting horizons are sometimes observed. Our many migrations indicate that here the deep crustal velocities (to ~30-35 km) are probably closer to those in Figure 3.3 than those in Table 2.

Composite 1-1A Line Depth Migration: WR Fault to 12 km Depth

Two different migrations are shown. The first migration (Figure 3.17) used our best estimate of the velocity structure based on well data (Figure 5). Figure 3.18 is an enlargement to show the WR thrust. The velocity model is the same as for line 1 and line 1A (Figures 3.3, 3.8). The sedimentary horizons at depth under the WR thrust appear to be depressed ~1 km. On the second depth section (Figure 3.19), created by a different velocity model (Figure 6), the sedimentary horizons

6 km	5.45 km/s
8 km	6.06 km/s
10.5 km	6.2 km/s
11 km	6.23 km/s
13 km	6.28 km/s
18 km	6.4 km/s
24 km	6.85 km/s
30 km	7.3 km/s
40 km	7.8 km/s
51 km	8.0 km/s

TABLE. 1. Interval velocity function which overmigrated line 1.

continue at a more or less constant depth in the sub-thrust region (the footwall), as illustrated by the reflector at 5 km depth. This migrated section was amplitude-balanced after migration. A close examination of the migrations and models shows that the faster sedimentary velocities (Figure 3.6) used to make Figure 3.19 "pushed" the sedimentary reflections on the far left side of the section deeper so that they "matched" the depth of their correlative events ***under*** the thrust.

If the deformation under the WR thrust is slight such that the formations continue approximately horizontally, then Figure 3.19 would appear to be the preferred earth picture. However, from the American Quasar dip-meter log (supplied by J.F. Parker), 40-50 degree N-NW dips are seen from 3.40-3.95 km, 3.98-4.27 km, and 4.41-4.54 km. These steep dips indicate that from 3.4-4.5 km depth, the deformation is not slight (and Figure 3.17 may be more accurate). Only a component of these high dips can be seen seismically because the line is running NE here. The complicated (3-D) geology in this particular zone makes conventional processing techniques practically invalid; thus the quality of the sedimentary stacked section is poor in the well vicinity. Another point favoring Figure 3.17 over Figure 19 is that the sedimentary velocities may be too high in the latter (Smithson, pers. comm.).

For comparison with Figures 3.17 and 3.19, the upper right corner of Figure 14 showing the (spliced) fit of migrated line 1 and line 1A is replotted in Figure 3.20. (The last 84 traces of line 1 are not shown there.) The entire figure is 1:1, with the traces of line 1A plotted

FIG. 3.14. Migrated line 1 (total section), using earth model in Figure 3.3. The ~8 km deep Green River Basin is seen; Time pullup in sediments under thrust is removed; the migrated syncline is clearly seen 6.8 km under arrow A; Pacific Creek thrust at arrow B; WR thrust along arrow C; arrow D points along the Continental Fault, a normal fault, part of the later Tertiary extensional deformation. Line 1's conversion from trace number [shown at top of sections to Stn. number (basemap): TR no. = 2 (Stn. - 2)]. Darker section (under km scale, and to the NE) is the spliced fit of the migrated line 1A to the migrated line 1.

FIG. 3.15. Migrated Pacific Creek anticline: line 1, 0.95 km, traces 110-410 (VE 1.3:1). ***Enlargement*** from Figure 3.14. Focused syncline may be faulted by Pacific Creek thrust. The lower 2 km of the Green River basin (mainly Paleozoic carbonates) are faulted; overlying Mesozoic sediments are folded (note better event continuity).

FIG. 3.16. Migrated WR thrust and underlying sediments: line 1, 0-9.5 km, tr. 410-710 (VE 1.3:1). ***Enlargement*** from Figure 3.14. Time pullup of sediments removed. Buckling, thrusting in sediments under granite suggested by seismic data. WR thrust along arrows. Below pt. A is a possible carbonate (reefal?) buildup.

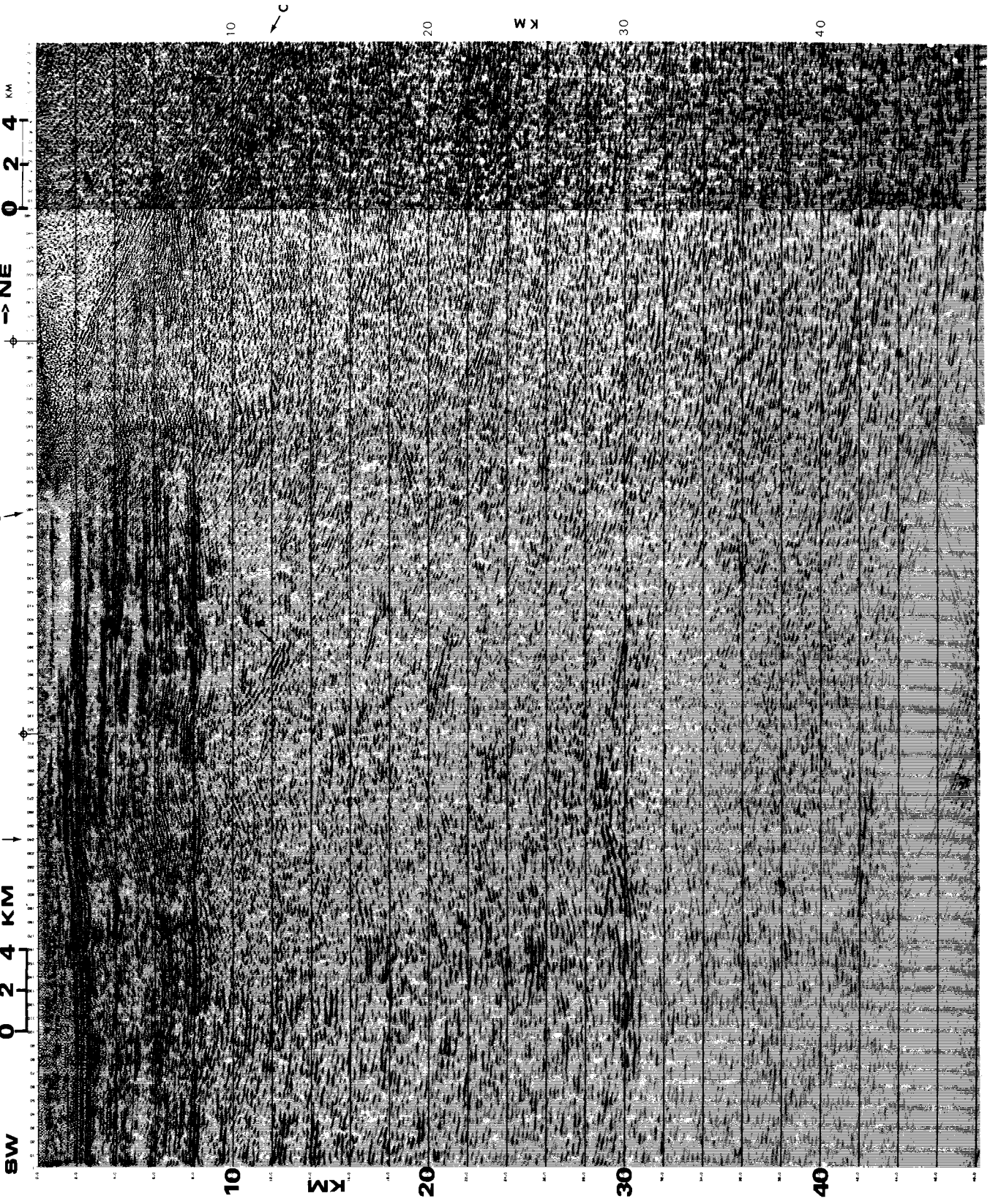

FIG. 3.14.

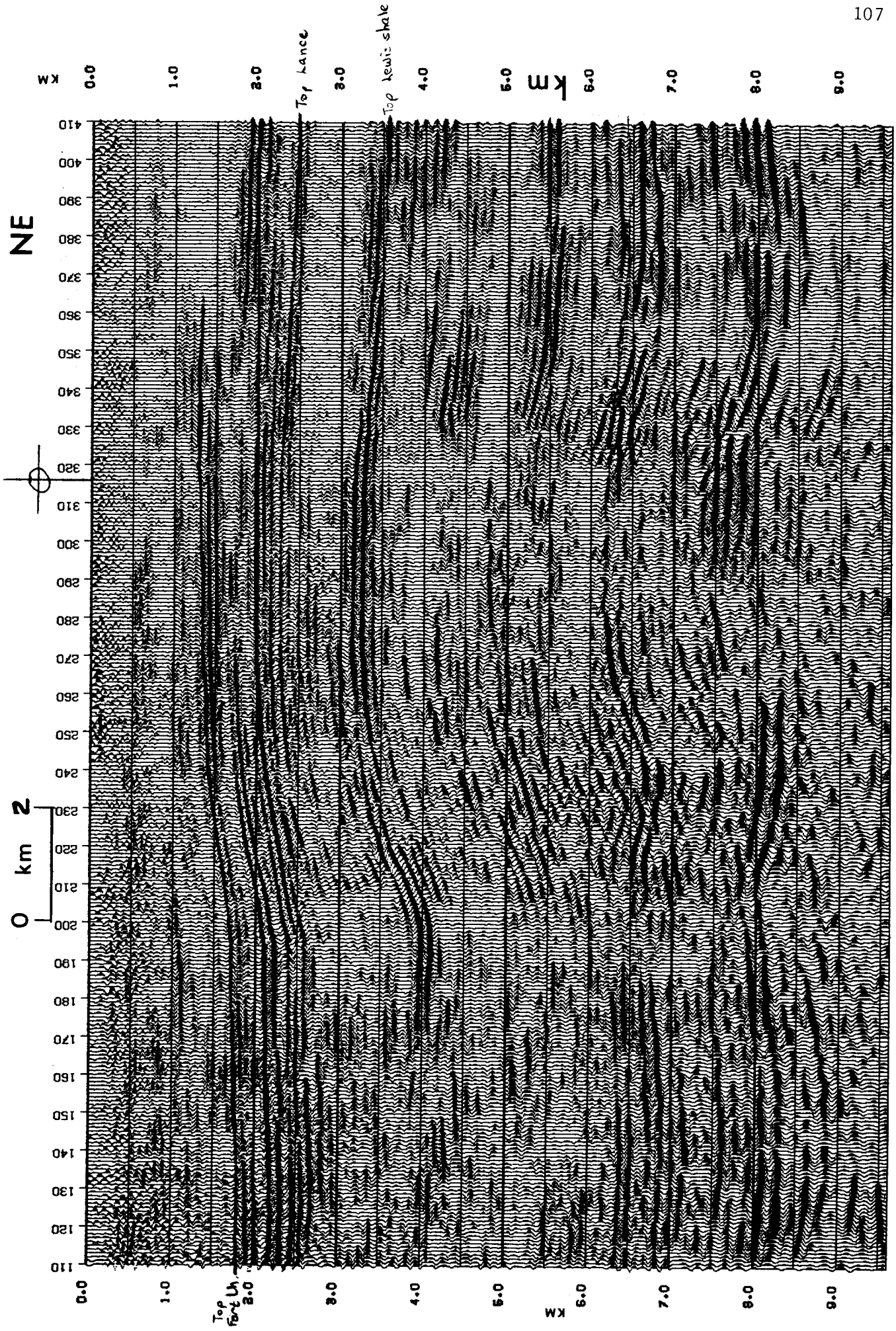
NE
0 km 2
Top Lance
Top Lewis shale
Top Fort Un
km
0.0
1.0
2.0
3.0
4.0
5.0
6.0
7.0
8.0
9.0

FIG. 3.15.

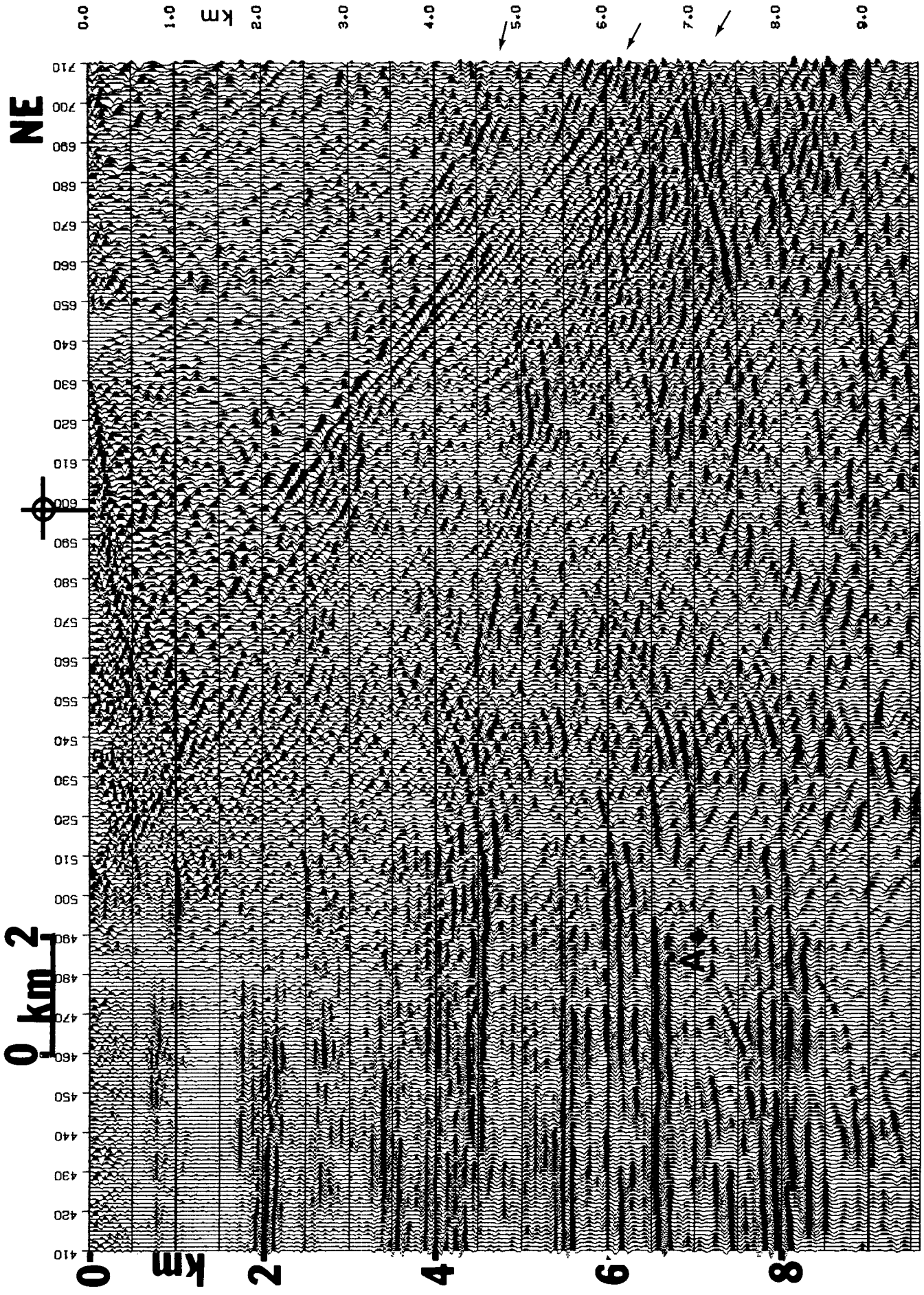

FIG. 3.16.

closer together because their trace spacing is 43 m (not 67 m like line 1). Since the first 150 stations of line 1A trend N15E, their projection to N55E results in the compaction observed on Figure 3.20.

Figures 3.17, 3.18, and 3.20, represent our best imaging of the WR thrust to 12 km depth. The lower horizons (4.5-9 km depth) in these figures also show the (possible) buckling and folding. The deep sedimentary reflectors (Figures 3.17, 3.20) appear to be depressed ~1 km deeper at the farthest point under the fault, perhaps by the load of the overthrust granite.

The highest amplitude fault reflections are at depths of 2-5 km. The fault is seen with a lesser amplitude from 0-1 km depth, and from 5 to ~11.5 km. Below ~12 km on Figures 3.17 and 3.19, due to the shortness of the input section, 20-30 degree NE dips will no longer be seen, as discussed in Chapter 1. The NE edges of the migrated sections will have no NE dipping energy. The steepest apparent dip observed in the upper 10 km of the fault is 32 degrees. On Figure 3.18 (at A), a 3 km long dip segment, a reflection from the WR thrust, clearly has a decrease of dip with depth at 6.6 km, going from a dip of ~30 degrees to a dip of a few degrees. The same event is seen on Figure 3.20 (A). Similar geometry within the fault zone is seen on Figure 3.17 at 3.5-4.5 km depth between traces 170-220 (C to C) and traces 200-250 (D to D). The apparent "bottom" of the fault zone is seismically a 3-legged dip segment at 9.8-10.8 km (traces 305-345, Figure 3.18; B on Figure 3.17) which displays the same style of decreasing dip with depth.

Line 1A Depth Migrations

Two migrated sections are displayed. In the first section, Figure 3.21, 16 sec from the time section was migrated, and the migration velocities came from geology and laboratory data. There is some indication of overmigration in the SW upper 5-10 km of the hanging wall, although that may be due to three-dimensionality or the line "straightening" process. In the second migrated section (Figure 3.22), seismic interval velocities (from dip-corrected stacking velocities and Dix's equation)

FIG. 3.17. Line 1-1A composite migrated section; earth model in Figure 3.3 used. Note first clearly seen shallowing/splay of WR thrust at 6.6 km depth (arrow A). Dipping reflection at arrow B is interpreted as being from the WR thrust. The sedimentary horizons at 4.5 km and deeper are depressed ~1 km, possibly by weight of upthrust basement. From C → C, and D → D, are similar geometries to that clearly seen at A, *i.e.*, a decrease of dip with depth.

FIG. 3.18. Migrated WR thrust: ***enlargement*** from composite 1-1A first migration (Figure 3.17). WR thrust along arrow. Pt. A shows the first obvious decrease of dip of the WR thrust (6.6 km depth).

FIG. 3.19. Alternate migration of line 1-1A. Sedimentary horizons are now subhorizontal under the thrust (see event at 5 km). This section was amplitude-balanced after migration.

FIG. 3.20. Migrated WR thrust: ***enlargement*** from Figure 3.14. Line 1's and line 1A's migrations were spliced together here; line 1A is darker because the trace spacing is smaller than line 1's. The entire figure is 1:1. Arrows point along WR thrust. Pt. A shows the first obvious decrease of dip of the WR thrust (6.6 km depth). From well data, reflection B is known to be from the top of the 1 km thick fault zone, and reflection C from the bottom.

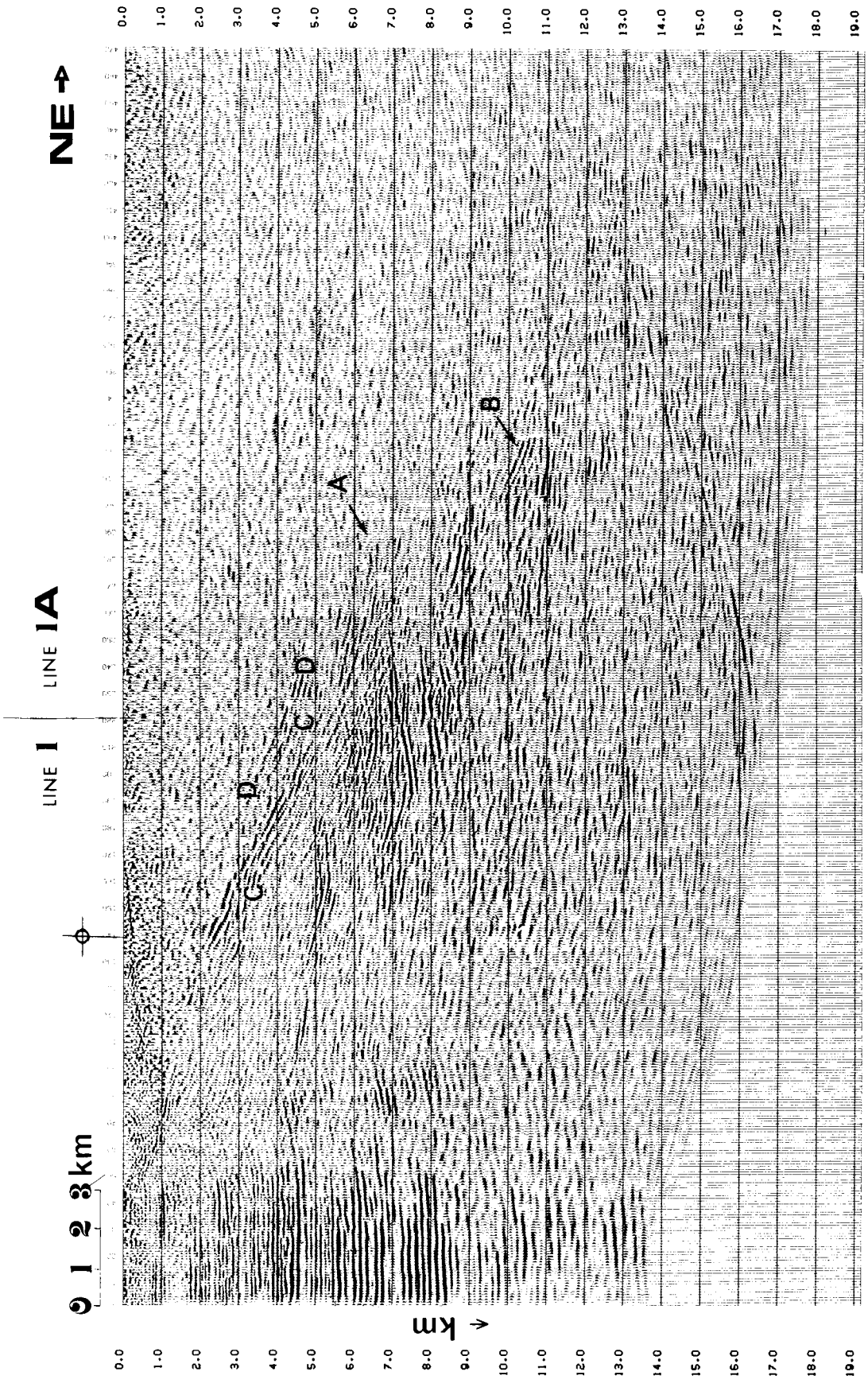
NE →
LINE 1A
LINE 1
A
B
C
D
0 1 2 3km
km
0.0
1.0
2.0
3.0
4.0
5.0
6.0
7.0
8.0
9.0
10.0
11.0
12.0
13.0
14.0
15.0
16.0
17.0
18.0
19.0

FIG. 3.17.

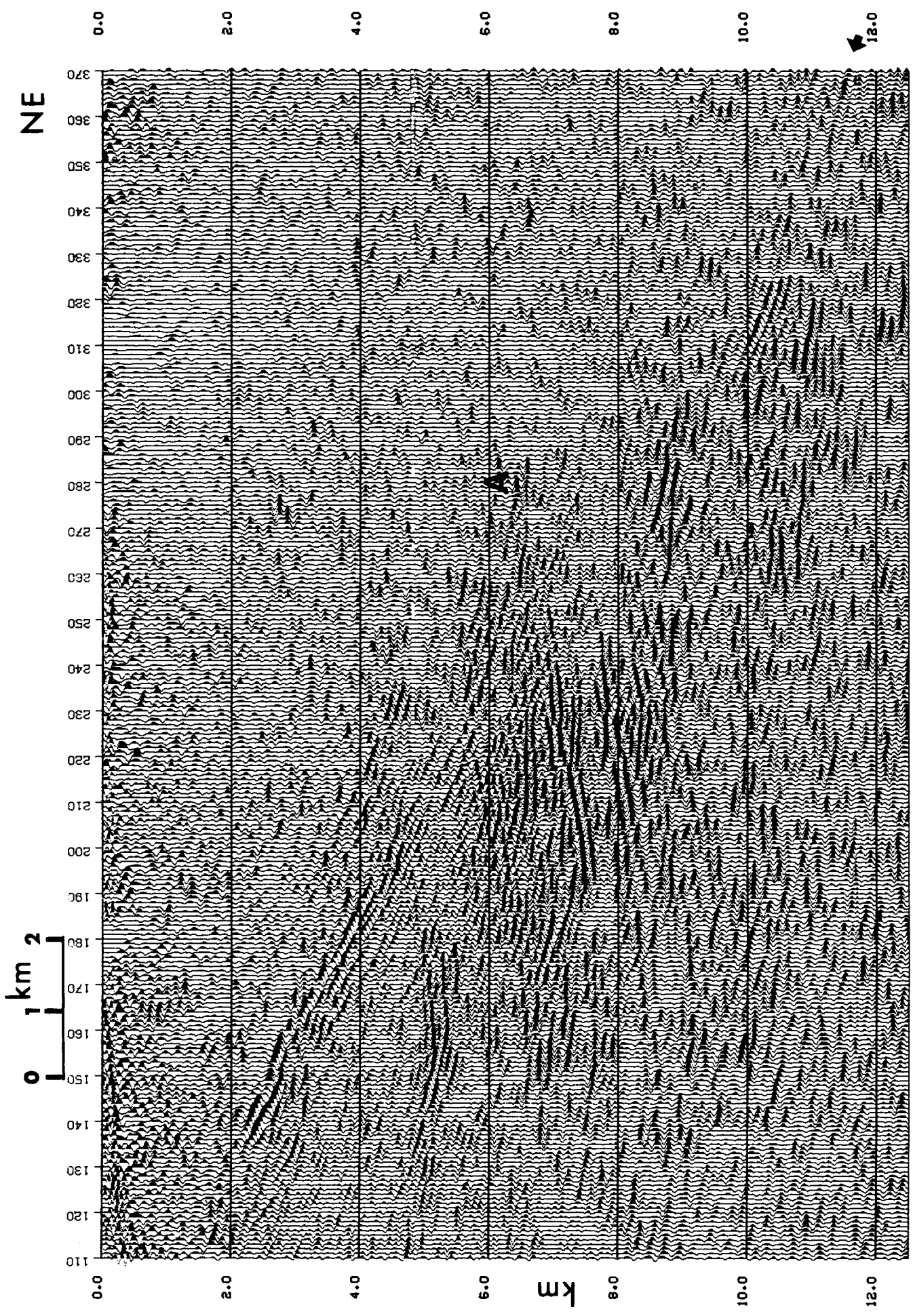
NE
0
1
km
2
0.0
2.0
4.0
6.0
8.0
10.0
12.0
km
110
120
130
140
150
160
170
180
190
200
210
220
230
240
250
260
270
280
290
300
310
320
330
340
350
360
370

FIG. 3.18.

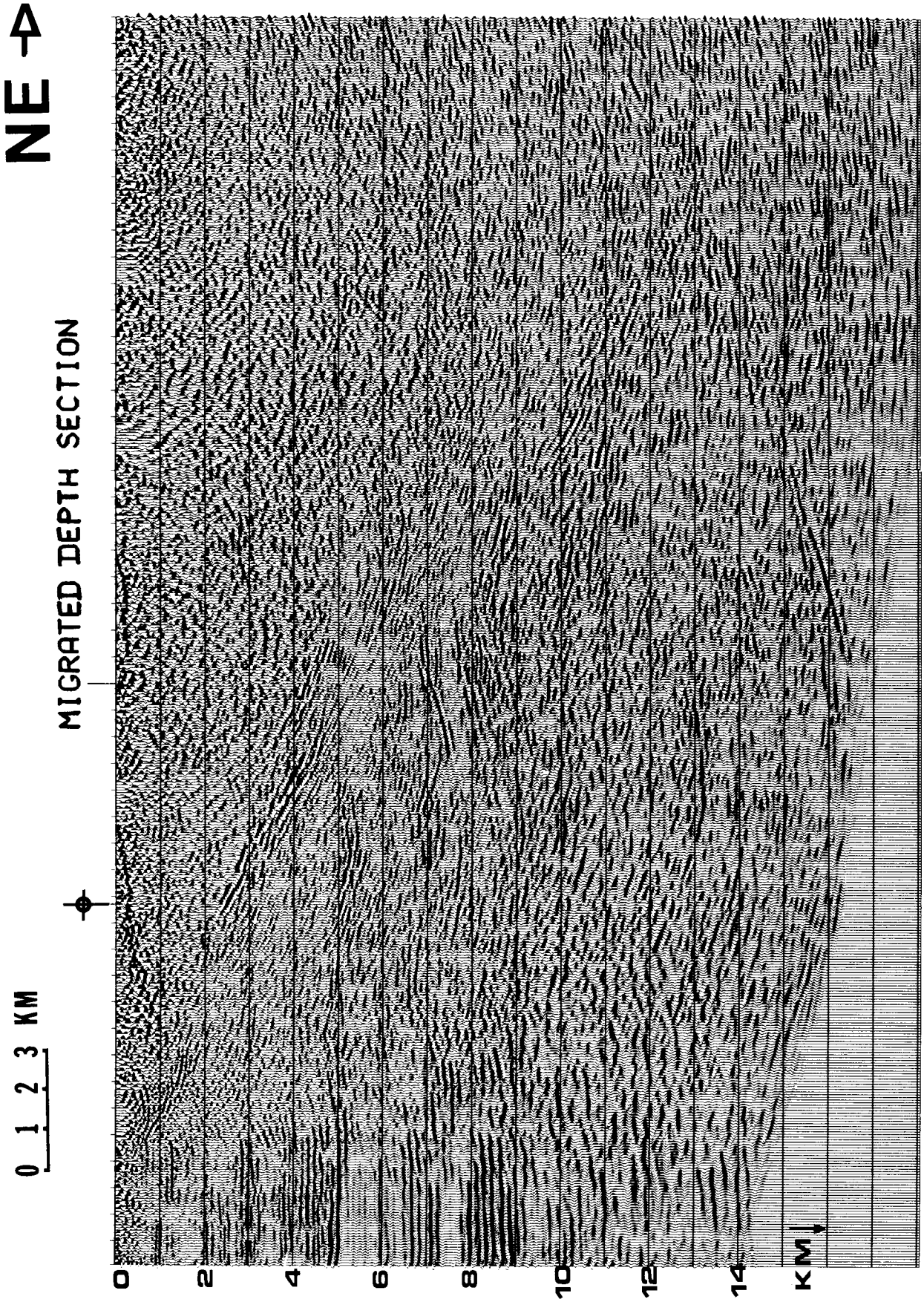

FIG. 3.19.

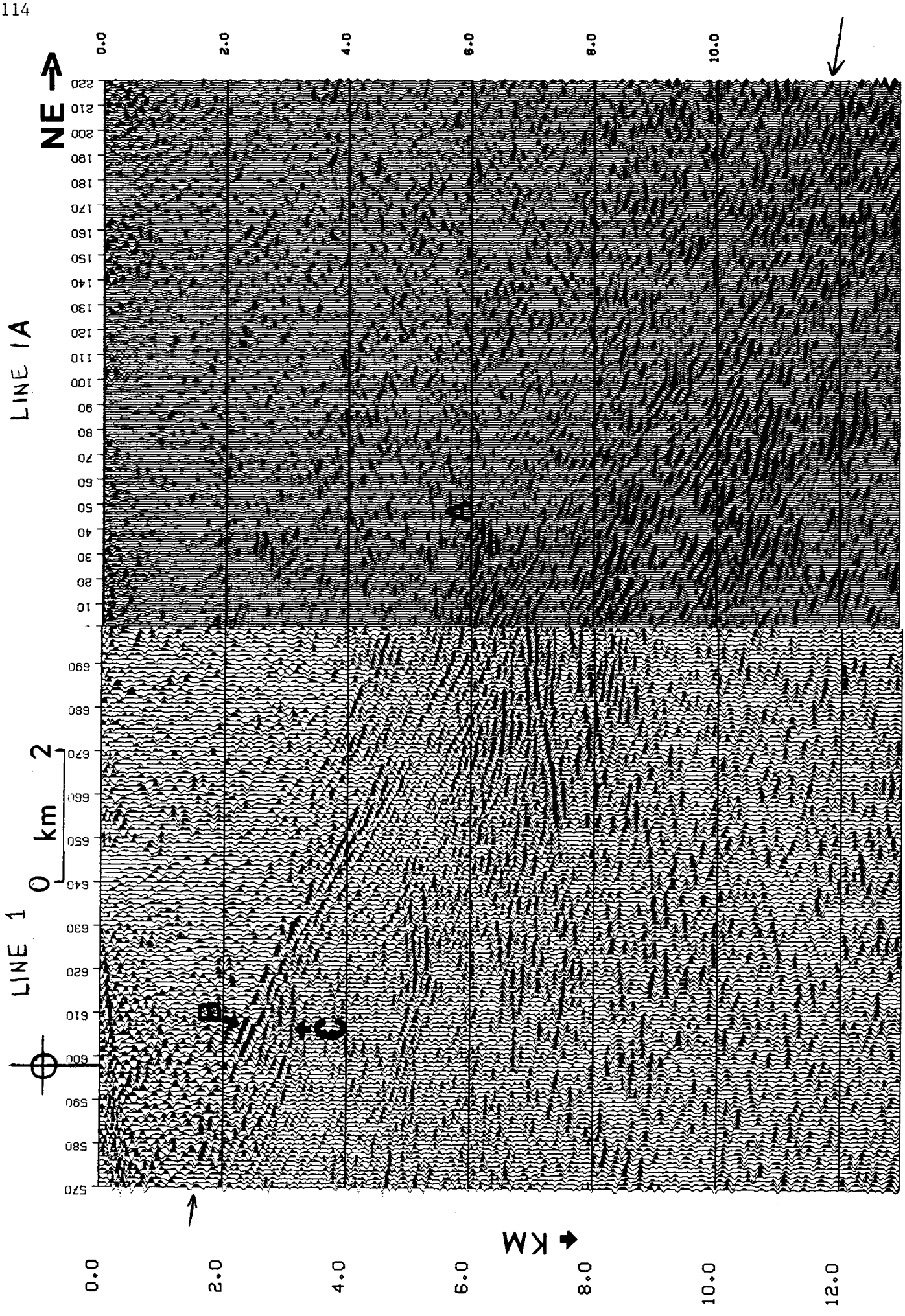

FIG. 3.20.

were used to migrate a portion (9.6 sec, ~25 km) of the non-projected line 1A. Note that the slower velocities in the upper 5-10 km or the lack of "straightening" resulted in apparently fewer overmigration artifacts than in Figure 3.21.

The structure of several major features was revealed by the migrations of line 1A. The WR fault can be traced on Figures 3.23 and 3.24, enlargements from Figure 3.21. 23-36 degree NE dipping energy which appears to be related to the WR thrust zone can be traced from 5 - 27 km depth. At 27 km depth, the lack of a longer input section cut short the reflections from the WR thrust. The apparent dip of the thrust is ~32 degrees. The complex structure of the fault zone is seen seismically as a series of dip segments which flatten with depth (Figures 3.20, 3.23, 3.24). The dip segments are ~2 km in length (concave upward). The thrust zone is ~6 km thick at 14 km depth (Figure 3.21). In the (interpreted) fault zone, strong bands of dipping energy at 18, 24, and 30 km depth flatten with depth. A deep crustal band of energy from 22 to 24 km depth (B, Figure 3.22) in the footwall under the thrust fault is composed of broken dip segments up to 2 km long. Energy similar in appearance occurs on the other side of the fault at depths of 14-16 km, 16.5-19 km, and 19.5-21 km (C, Figure 3.22). In the upper 5 km on the SW part of line 1A (in the hanging wall), the Precambrian rocks are for the most part seismically transparent. The basement 5-8 km away from the WR thrust contains two zones of gently dipping, concave-upward fairly continuous reflectors (C, D, Figure 3.21; D, E, Figure 3.22). In the lower center of the line (32-45 km depth, Figure 3.21), a zone of deep crustal reflectors is seen.

Composite 1A-2 Line Depth Migration (16 sec, ~50 km depth)

The composite migrated 1A-2 line fills in the gap of WR fault reflections at the end of line 1A (last 300 traces, >27 km depth, Figure 3.21). The following features are exhibited (Figure 3.25). The WR basinal sediments thicken to the NE; the Derby Dome is seen at C, Figure 3.25. The line runs nearly along strike here. The base of sediments is not always clearly seen. Within the upper Precambrian crust, four

FIG. 3.21. Projected line 1A migrated. WR thrust seen along arrows from 2-27 km depth (at which point the reflections end due to the shortness of the input section). Letters A and B show the zone of crustal reflectors interpreted as offset by the fault. Letters C and D show the upper crustal reflectors which may be thrust faults. Due to projection of crooked seismic line onto straight line, exact conversion from trace no. to stn. no. is not possible.

FIG. 3.22. Alternate migration of part of line 1A; the migration used slower velocities to 6 km depth. The last ~200 traces of line 1A (and the important NE dips contained therein) were ***not*** included in this, the shorter of the 1A migrations. These dips were included in the input to the large (complete) migration of line 1A (Figure FIG. 3.21). WR thrust is seen along arrows A; note high-amplitude reflections from the interpreted base of the WR fault zone at A. The zone of reflectors at 21-24 km depth (location B) is interpreted as offset 6-8 km by the WR thrust at 22 km depth. The continuation of zone B is zone C (15-17 km depth, shaped like a horseshoe lying up on edge). Arrow D and E point along upper crustal reflections which are speculatively interpreted as thrusts. The difference in upper-crustal migration velocities was 6.0 km/s (Figure 3.21) vs. 4.5 km/s (Figure 3.22). Slower velocities appear to have imaged the data better; perhaps the tremendous amount of movement along the fault zones has very effectively fractured the upper crustal granite (0-5 km depth) such that 4.5 km/s is the imaging velocity.

FIG. 3.23. Migrated line 1A: ***enlargement*** of Figure 3.21 from 12-24.5 km. Arrows point along the WR thrust. Location A is the zone of crustal reflections (22-24 km depth).

FIG. 3.24. Migrated line 1A: ***enlargement*** of Figure 3.21 from 18-31 km, shows the end-of-line effect compared to Figure 3.26. Arrows point to WR thrust.

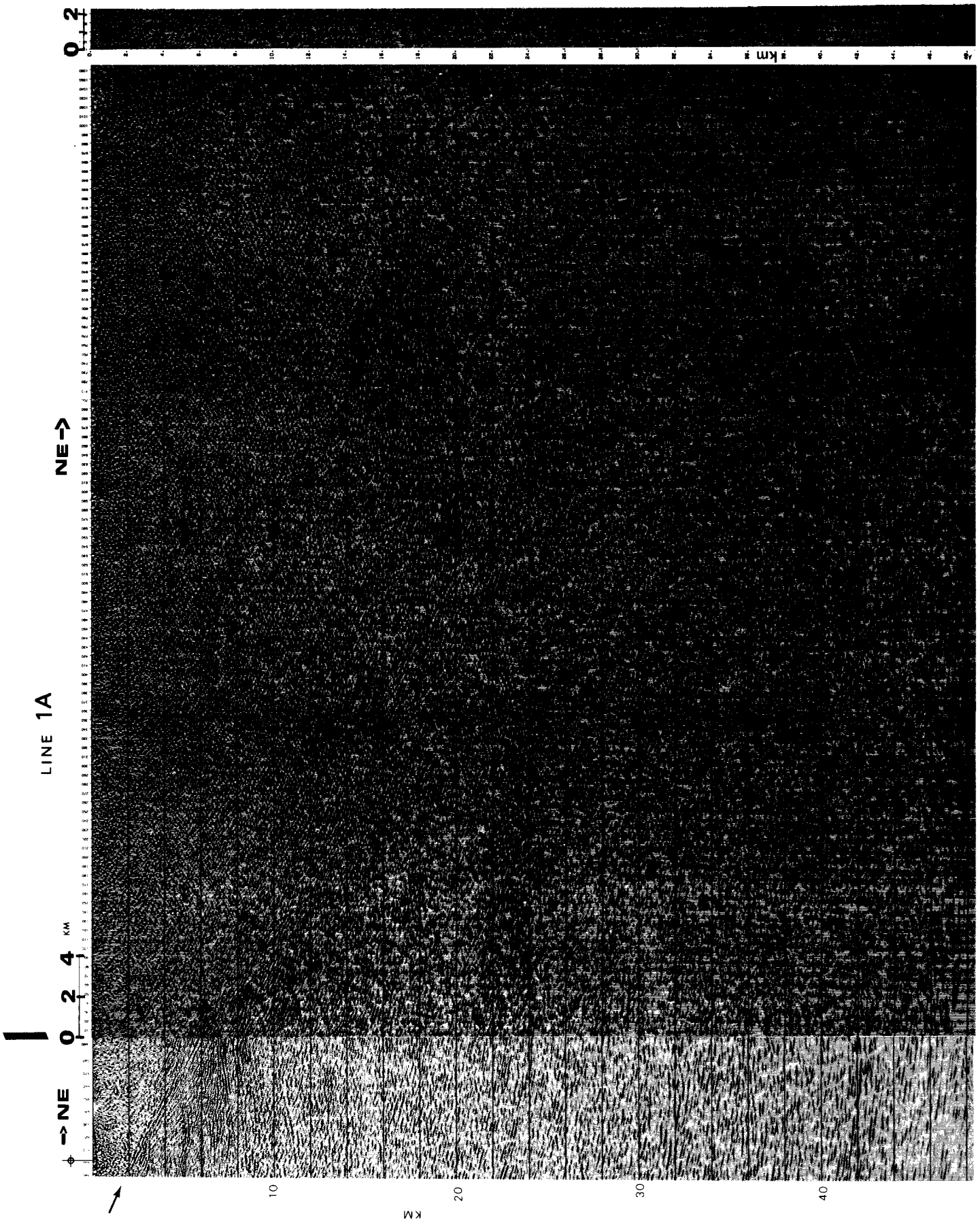

FIG. 3.21.

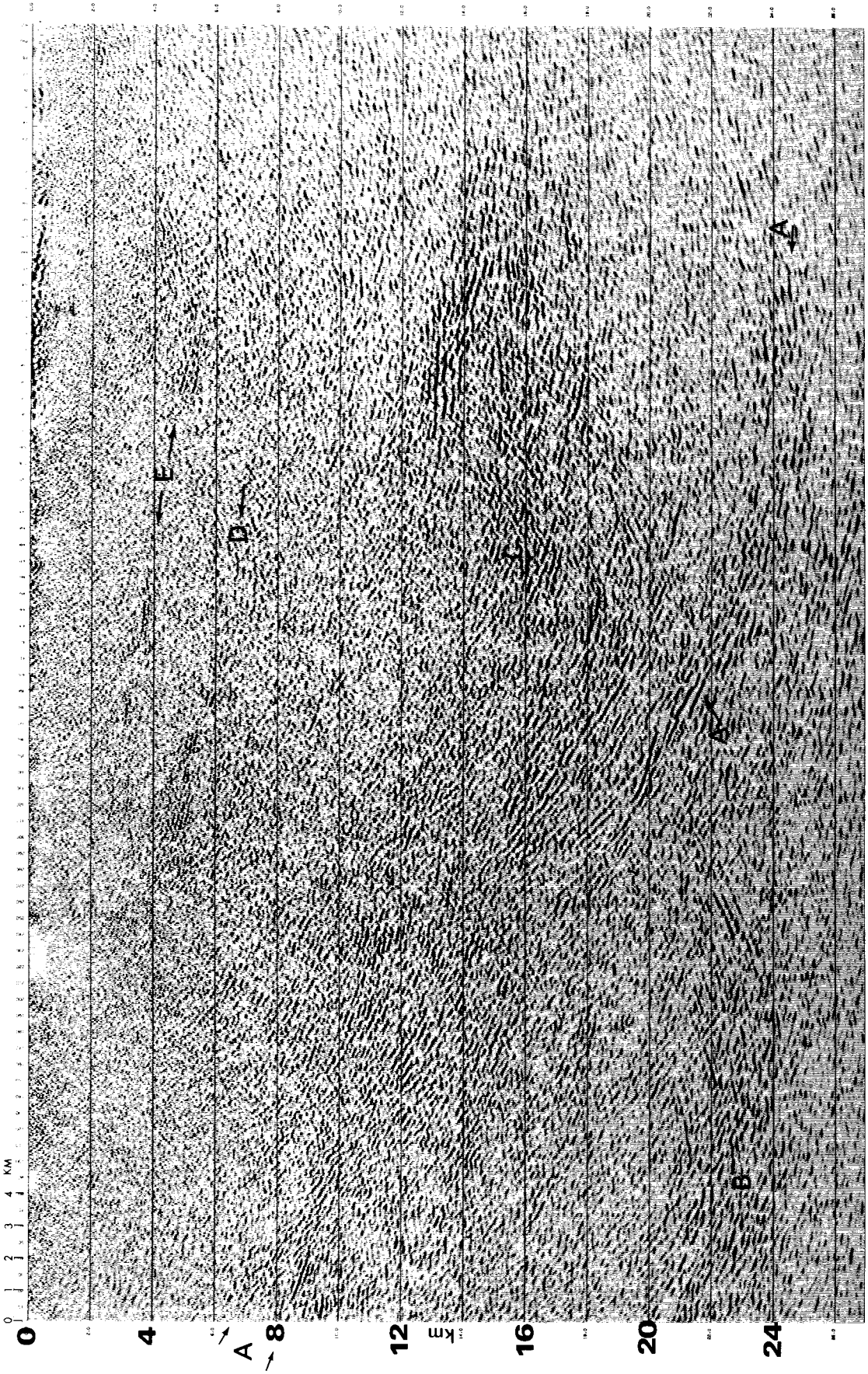

FIG. 3.22.

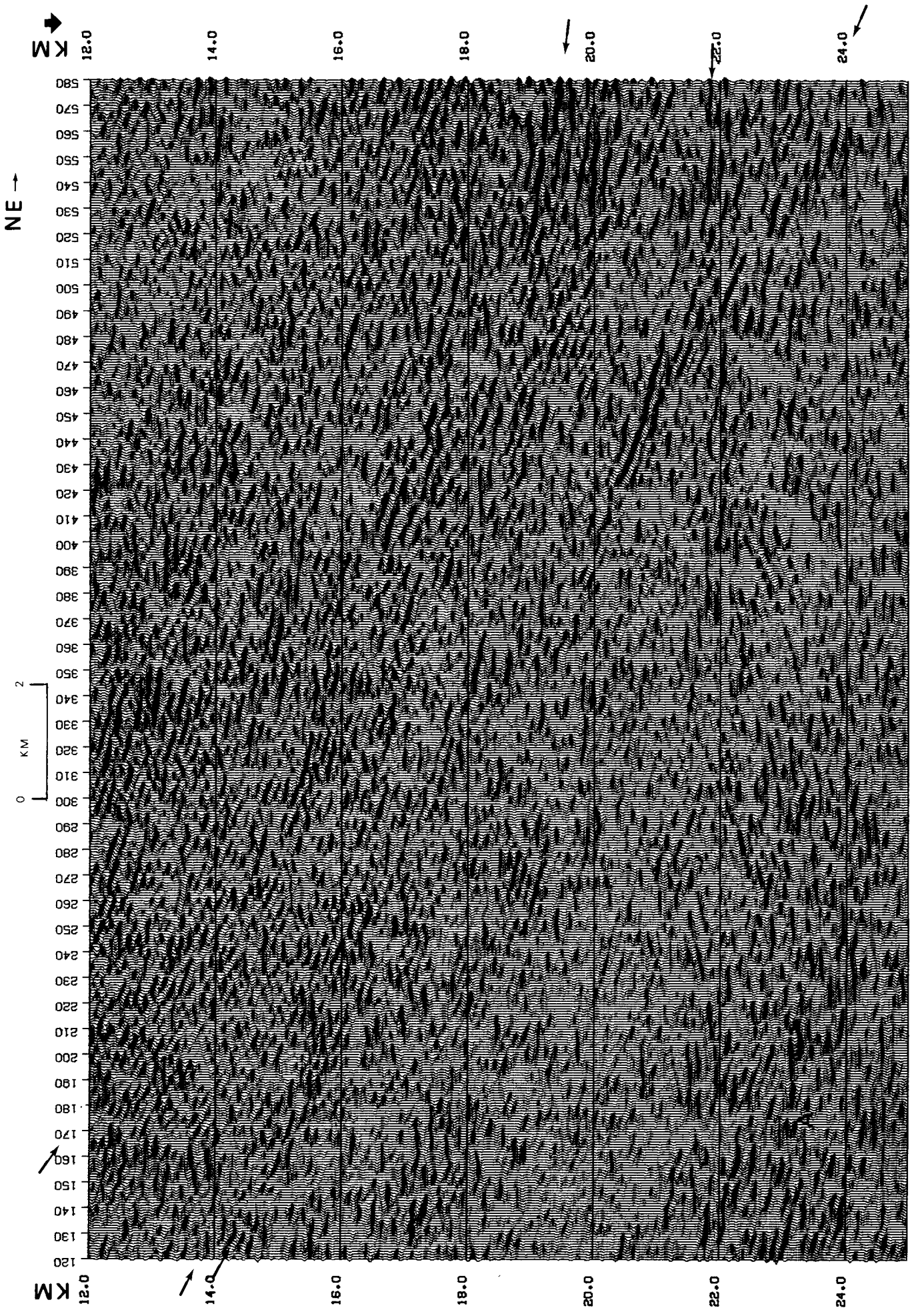
KM
12.0
14.0
16.0
18.0
20.0
22.0
24.0
NE
580
570
560
550
540
530
520
510
500
490
480
470
460
450
440
430
420
410
400
390
380
370
360
350
340
330
320
310
300
290
280
270
260
250
240
230
220
210
200
190
180
170
160
150
140
130
120
0
KM
2

FIG. 3.23.

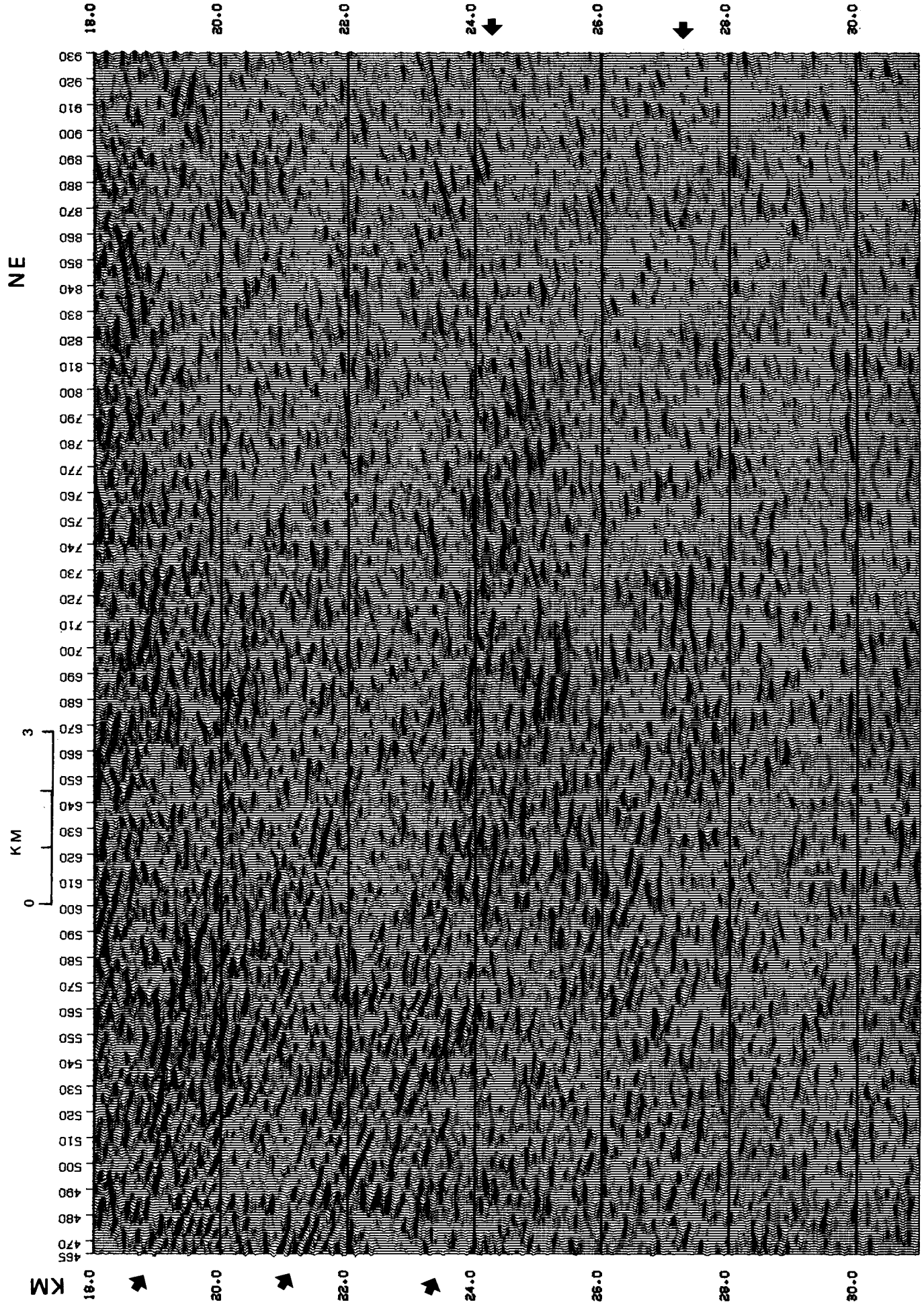
NE
KM
0
3
18.0
20.0
22.0
24.0
26.0
28.0
30.0
930
920
910
900
890
880
870
860
850
840
830
820
810
800
790
780
770
760
750
740
730
720
710
700
690
680
670
660
650
640
630
620
610
600
590
580
570
560
550
540
530
520
510
500
490
480
470
465

FIG. 3.24.

gently dipping zones of reflections cross the section. The most prominent reflections within the crystalline crust are those from 13-17 km depth (D, Figure 3.25). They have the appearance of part of a recumbent fold (similar to a horseshoe lying upright on its side with the top edge broken off). Another dipping zone of reflectors lies between 17 and 21 km depth in the center of the dataset (E, Figure 3.25). It is not apparently connected with the energy at 13-17 km depth.

A quite interesting artifact of the migration is seen at 19-20 km depth (along arrow B, Figure 3.25): it has SW dip on the SW edge of the line, which is ***not*** possible for a geologically caused reflection (see Chapter 1). The artifact was caused by imperfect absorbing boundary conditions. The unmigrated data show its premigration location--a high-amplitude NE dipping reflector (in segments) from 7-8 sec (tr. 20-160). When this energy was migrated updip, most of it was absorbed by the boundary, but some energy ***was*** reflected off the boundary and bounced back onto the section. The correctly migrated position of this energy is shown on Figure 3.21 at 20.5 km depth (tr. 410-470, below C and slightly to the left).

The continuation of the WR fault may be observed in the enlargements (Figures 3.26, 3.27) of Figure 3.25. Figure 3.26 displays on the left a repeat of migrated line 1A again (from Figure 3.21); on the right is the migrated 1A-2 line (from Figure 3.25). The break in trace numbering indicates the junction of the two datasets. There are NE dipping reflectors at 20-22 km depth (arrows, Figure 3.26, tr. 1-100), and at 28-32 km (arrows, Figure 3.27, tr. 280-680). In these zones, the dips decrease with depth, suggesting flattening of the thrust fault. Figure 3.27 shows a 4 legged high amplitude dipping reflection (31.2 km, tr. 335-360) that appears to be part of the WR fault. The lack of adaptive deconvolution (as compared to Figure 3.28) is noticeable.

FIG. 3.25. Projected line 1A-2 migrated section. WR thrust along arrows A; at arrow B, migration artifact (energy reflected from not completely "absorbing" boundary). WR basin sediments seen in upper right corner. C marks the Derby Dome; D marks the large recumbent fold in the crystalline crust; the letters E point along a dipping zone of upper crustal reflectors.

FIG. 3.26. Migrated line 1A and line 1A-2 spliced together: 18-31 km, removing the end-of-line effect seen in Figure 3.19. Arrows point along WR thrust. ***Enlargement*** from Figures 3.21 and 3.25.

FIG. 3.27. Migrated line 1A-2: ***enlargement*** of Figure 3.21, from 21-34 km. Arrows point along WR thrust.

FIG. 3.28. Migrated line 2. Arrows point along WR thrust. Location A is the Sand Draw anticline, probably underlain by a thrust (not seen seismically). To convert between trace no. (shown here) and stn no. (basemap), tr. no. = 2 (stn. - 3.5) . Three different subhorizontal bands of crustal reflectors are marked (B,C,D).

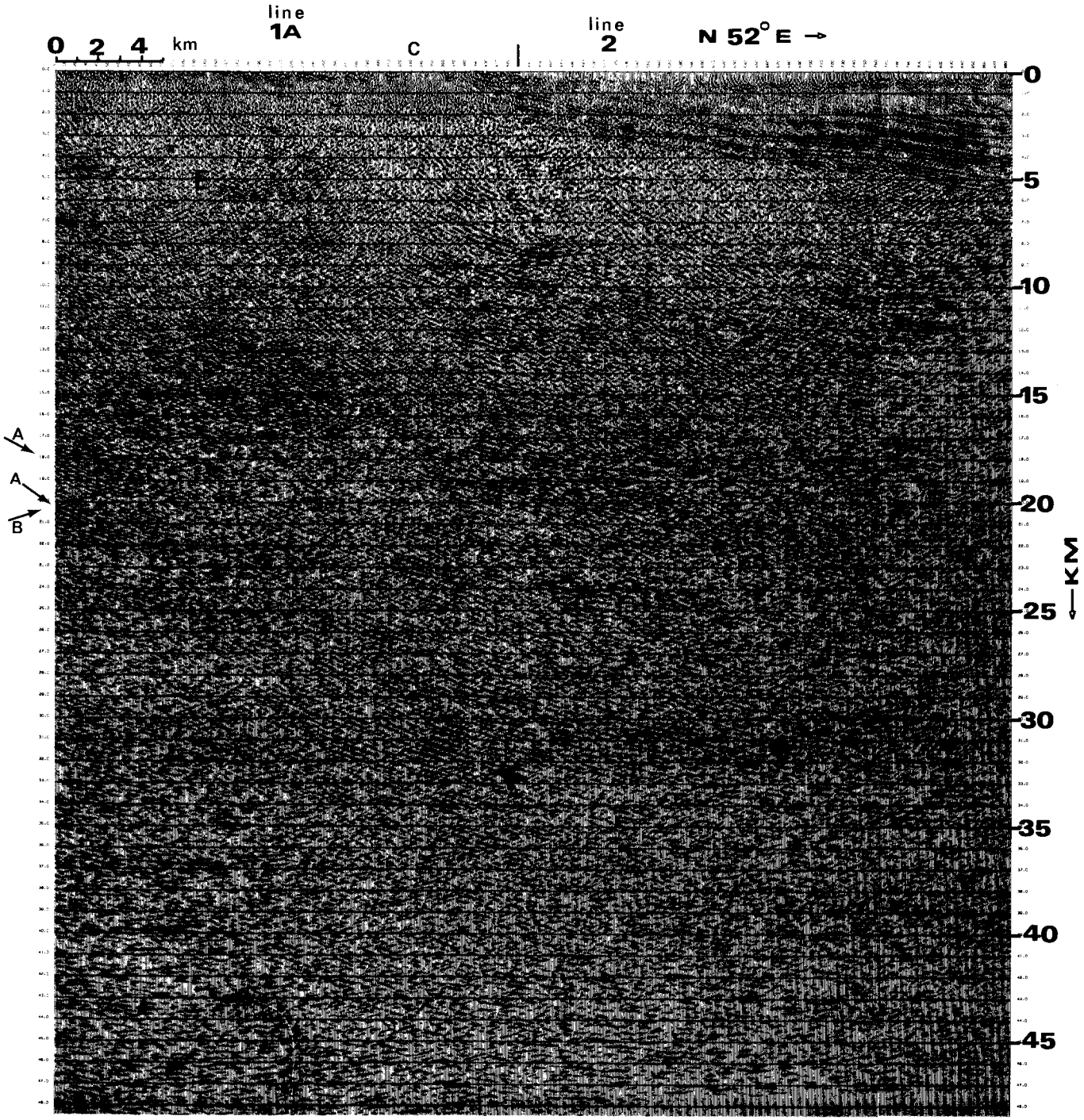

FIG. 3.25.

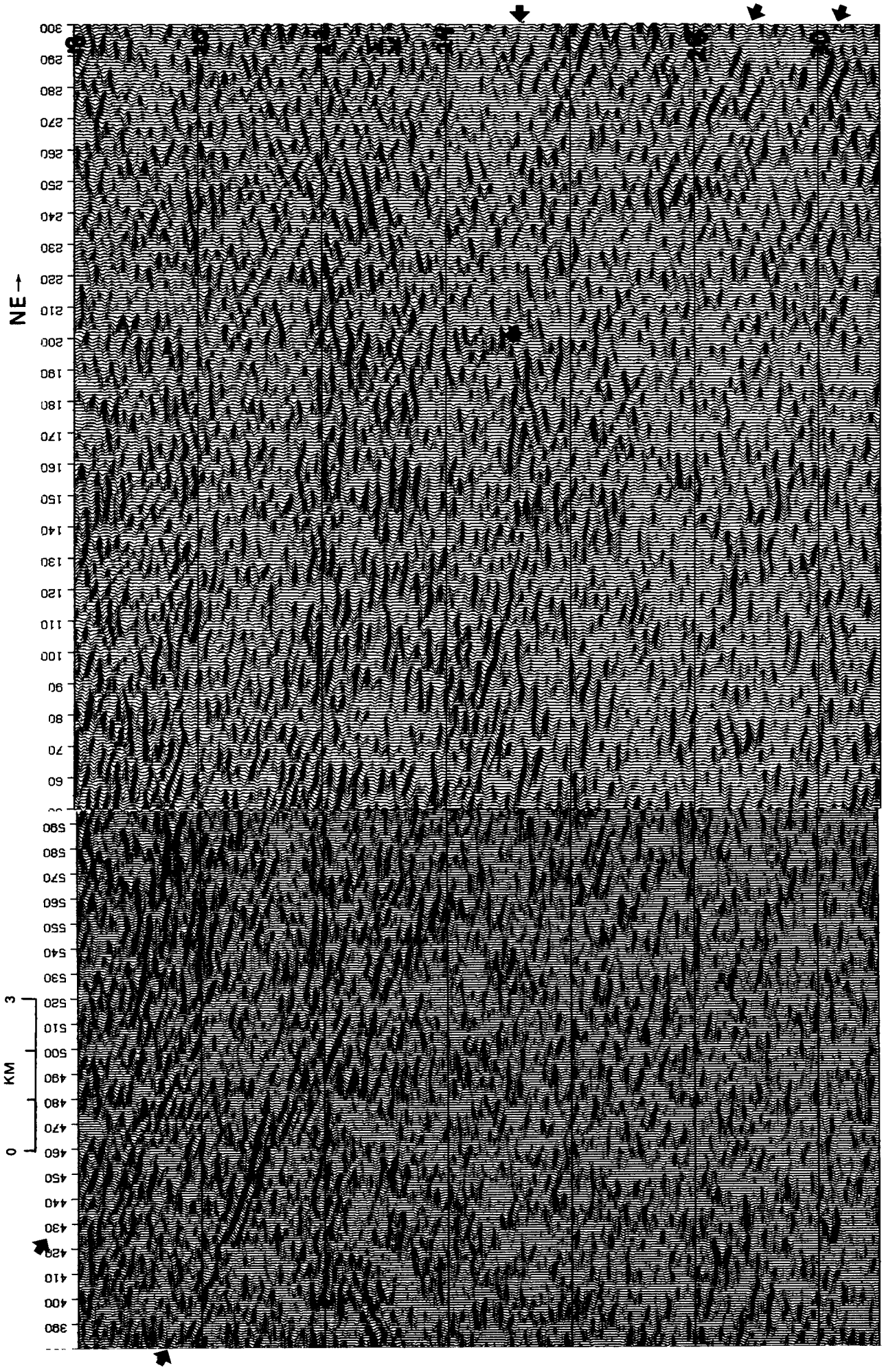

FIG. 3.26.

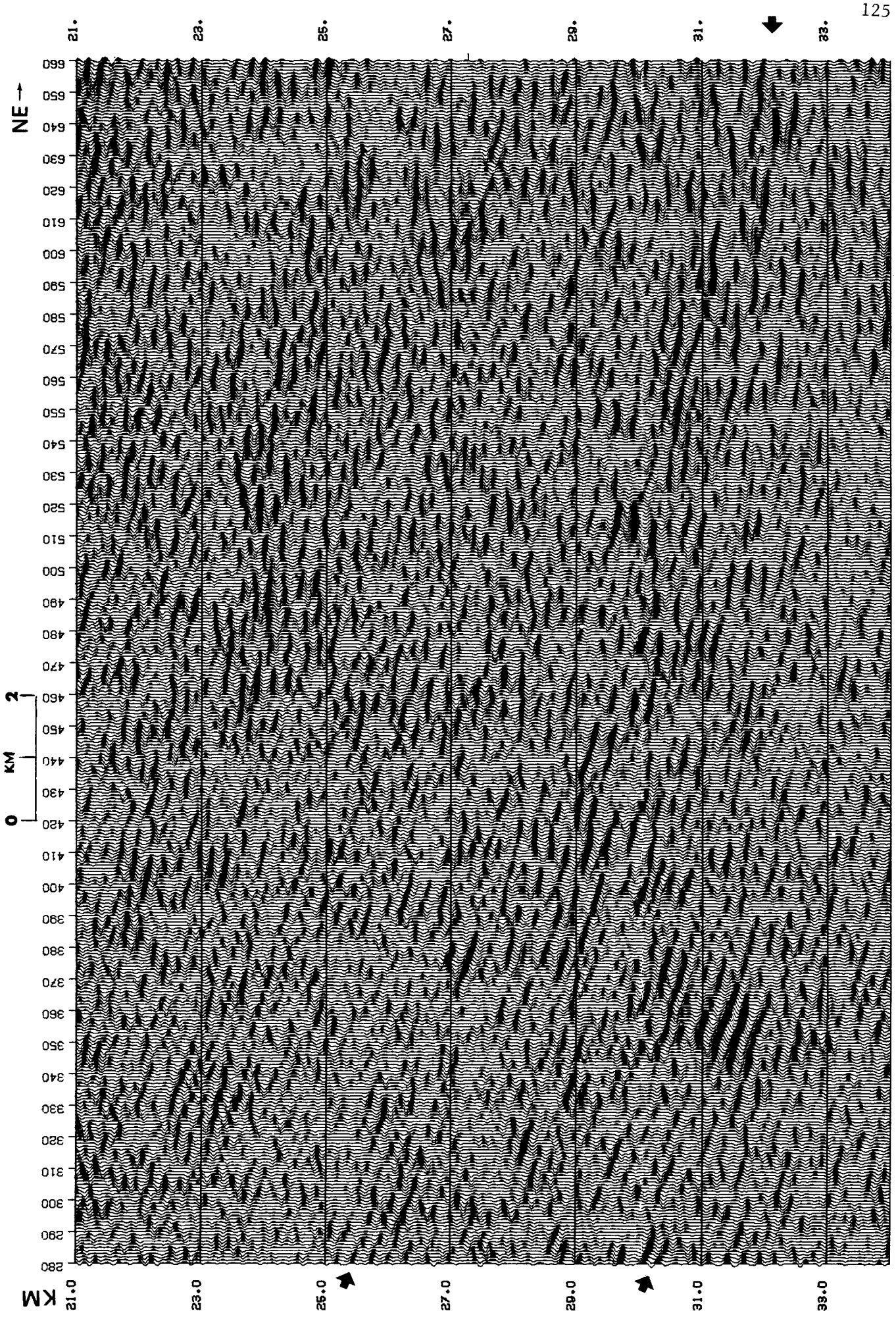
21.
23.
25.
27.
29.
31.
33.
NE
660
650
640
630
620
610
600
590
580
570
560
550
540
530
520
510
500
490
480
470
460
450
440
430
420
410
400
390
380
370
360
350
340
330
320
310
300
290
280
0
KM
2
KM
21.0
23.0
25.0
27.0
29.0
31.0
33.0

FIG. 3.27.

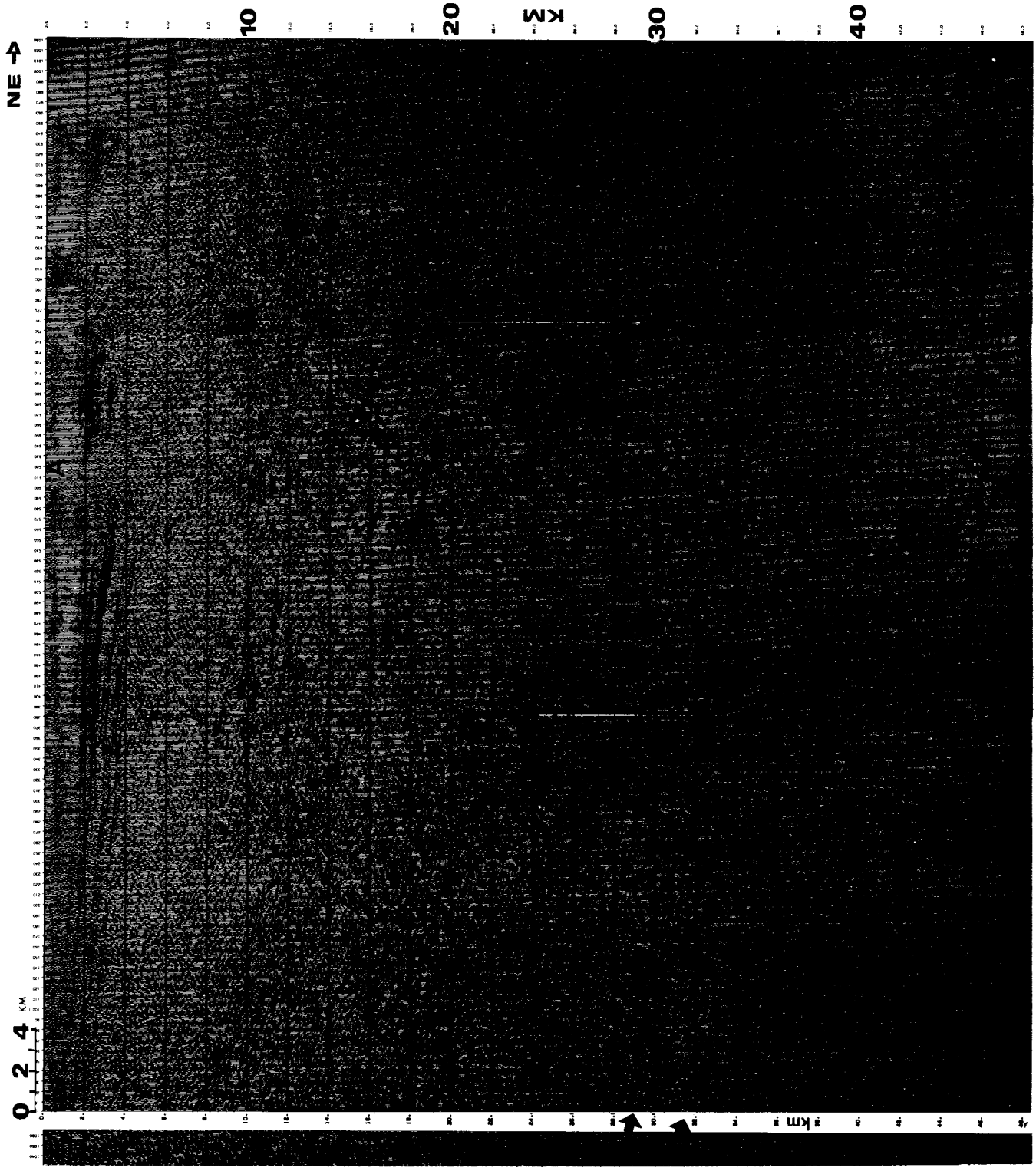

FIG. 3.28.

Line 2 Depth Migration (16 sec, ~50 km depth)

The deconvolved migrated line 2 (Figure 3.28) reveals zones of higher amplitude reflections, and a comparatively transparent central section. The data present these features: the deepening of the WR basin; three thrust faults offsetting the sedimentary layers; and three different subhorizontal bands of intra-crystalline crustal reflectors. The upper subhorizontal band of energy dips to the NE from 8-9 km depth in the west to 12-13 km in the east (arrows B, Figure 3.28). The middle band of NE-dipping energy extends from 17 to 19 km depth (SW) to 18-20 km depth (NE) along arrows C, Figure 3.28. The lowest band of energy centers around 29-32 km depth, and is seen only in the SW third of the line (arrow D, Figure 3.28). The Sand Draw anticline (A, Figure 3.28) is evident in the seismic data by the offset of the sedimentary layers and is a producing oil field.

More reflectors are seen in the SW part of the line than in the middle or in the east. (A good number of those reflectors have NE dip.) The relatively transparent zone seen in the middle third of the migrated line is puzzling. It may be due to sub-optimum processing, or to a (geologic) lack of reflectors, or to unusual scattering in the "near surface" (the thrust fault in the middle of the line), which prevents the transmission and return of coherent energy.

BRIEF REVIEW OF GEOLOGIC SETTING

The basement rocks of Wyoming are complexly deformed Archean crystalline rocks of varying composition, and range in age from 2.3 to more than 2.7 b.y. (Blackstone, 1963). Younger crystalline rocks (1.5-1.8 b.y.) are present in Utah and SE Wyoming. The WR uplift may be described as an asymmetric thrust-faulted anticline which plunges doubly to the NW and SE, the latter direction toward the COCORP line across the southern part of the range. The more deeply eroded central part of the range reveals lower crustal pyroxene granulites, progressing southeastward to supracrustal gneisses and intrusive granites. Near the COCORP

line, a zone of shearing (Precambrian suture zone?) separates intrusive granites (north) from strongly folded supracrustal gneisses and schists (meta-ironstone, meta-andesite, and metagraywacke, Bayley *et al.*, 1973).

The Paleozoic section in the Green River and Wind River basins is dominantly marine, with resistant limestone and dolomite being more abundant than the sandstones and shales. Since shallow seas covered central Wyoming from early Paleozoic through most of Mesozoic time, slight fluctuations in a mostly stable tectonic environment did produce offshore, nearshore, shoreface, and intertidal deposits (Keefer, 1970). The Mesozoic section is mostly shale, siltstone, and sandstone. Changes in the balance between subsidence and sedimentation produced four major transgressive-regressive cycles and complex intertonguing of swamp, shallow water, and flood plain deposits.

In latest Cretaceous (Lance time), the Laramide orogeny began, possibly triggered by a change to shallow subduction along the western No. American margin. The GR and WR basins were separated at this time by uplift on the WR thrust. Terrigenous sediments were shed from the rising mountain ranges and deposited in the subsiding basins. Fluvial and lacustrine deposition ensued. Deformation apparently ended by late Early Eocene.

Classic Laramide deformation has been described as asymmetric thrusted-anticline "uplift" of basement blocks, accompanied by active subsidence of the adjacent blocks (Keefer, 1970). The migrated WR data suggest that the transport of the WR mountain block was along a fault plane with an apparent dip of 30 degrees to ~32 km depth. True dip may be as much as ~40 degrees (Smithson, pers. comm.). Laramide deformation is seen as brittle and concentrated along the edges of the blocks (Kanter, *et al.*, 1979). The deepest part of the basins are generally adjacent to the highest parts of the uplifts.

Later Tertiary sediments are clastics with increasing amounts of volcanic debris. Post Eocene extensional faulting is most intense to the west of the GR basin. The seismic data also show normal or extensional faulting, in front of the WR thrust, associated with the mapped Continental fault. More detailed discussions of Laramide structures and

the geologic history of Wyoming are found in the extensive literature.

INTERPRETATION

A primarily structural interpretation of the most significant features on the migrated sections comprises this section. Detailed lithologic or stratigraphic interpretations in the Precambrian or Phanerozoic rocks will not be discussed in this paper. Major features portrayed in the migrated data are the Pacific Creek anticline and the WR thrust.

The Pacific Creek Anticline and the Green River Basin

Stratigraphy. An analysis of formation thickness over the Pacific Creek anticline can yield the timing of anticlinal growth. If depositional thinning in identifiable horizons over the anticline is observed, then the anticline would have already been topographically high during that time. The following picks of the formation tops in the Superior Oil Pacific Creek Unit No. 1 (Sec. 27, T27N, R103W) were used (from Hayes, 1977):

	depth	*two-way time*
T Top Fort Union	1.34 km	0.753 sec
K Top Lance	2.31 km	1.297 sec
K Top Lewis	3.28 km	1.717 sec
K Top Mesa Verde	3.55 km	1.865 sec
K Top Baxter	4.83 km	2.503 sec
K Top Frontier	6.01 km	3.053 sec

TABLE. 2. Formation picks in the Superior Pacific Creek No. 1 (from Hayes, 1977).

The time-to-depth function came from the well velocity survey and the sonic log; the values are corrected to the seismic datum of 6700 feet. The first evidence of thinning is in the Upper Cretaceous Lewis shale: the Lewis shale appears to be 200 m thicker at the ***start*** of line 1. However, this thickening is seen on the SW edge of the line 21 km (13 miles) away from the anticlinal crest and may be due to proximity to the depocenter, and not to growth of the anticline. A thickening of 350 m in the overlying Lance shale (latest Cretaceous) was observed directly to the SW of the Pacific Creek anticline. 300 m of the thickening is clearly observable to be in the ***base*** of the Lance shale, indicating that the anticline had formed by ***earliest*** Lance time. A thickening of 150 m in the Paleocene Fort Union is seen to the SW of the anticline. Above the Fort Union, picks were more difficult. Dating of the PC thrust as Earliest Lance (Latest Cretaceous) indicates it to be a Laramide feature, which is not surprising.

If thickening in identifiable Upper Cretaceous - Paleocene GR Basin horizons in front of the WR thrust (due to proximity of source) can be observed, dating of that thrusting will be possible. Unfortunately, we were not able to follow horizons northeastward from the PC anticline to in front of the WR thrust. Careful reprocessing of the data will hopefully enhance event continuity such that detrital wedges at the toe of the advancing thrust can be observed.

The Baxter shale (middle Upper Cretaceous) was 400 m thicker over the anticline than on the SW edge of the line, indicating probably that the depocenter in Baxter time was closer to the center of line 1.

A feature resembling a carbonate platform or reef is seen at (A), Figure 3.16 at 7.2-7.6 km depth (tr. 460-540). SW dip at 7-7.7 km (traces 460-480) in an otherwise horizontal sedimentary section, is followed by NE dip (traces 500-540). This lower section of the Green River (GR) Basin is dominantly Paleozoic carbonates.

Structural. The PC thrust's effect on the Green River basin sediments is shown on the migrated data. The dominantly carbonate lower Paleozoic horizons were faulted and folded, and continuity of seismic events is poor; the upper horizons (Mesozoic - Paleocene) were folded,

not faulted, and event continuity is significantly better.

The base of sediments under the thrust is probably represented by the group of reflectors at 8.2-9.0 km (Figures 3.19-3.21); the dipping reflector at 9.2-10.5 km may be the base of the WR fault zone. The layered reflectors at 10.5-11 km may be a repeated section of Madison limestone with the overlying 2 km section. As compressional forces grew in latest Cretaceous time, the lower sedimentary section may have been repeated by faulting along a SW dipping thrust plane, before (or during?) the formation of the WR thrust, as shown in Figure 3.29.

The Wind River Thrust and the Pacific Creek Thrust

The geometry of the WR thrust is of utmost importance to an understanding of Laramide tectonics. A steep or vertical fault plane would imply vertical uplift of the WR Range. The ~30 degree apparent dip of the fault zone implies predominantly horizontal movement. If its dip decreases with depth, or if there were splaying members of the thrust which decrease in dip with depth, then tilting of the hanging wall block and its overlying sediments (WR basin) would occur. If the fault's dip remains constant with depth, then no tilting would be expected. The WR basinal sediments are tilted, and so the interpretation and mechanism of the WR faulting must take that fact into account.

Before interpreting the seismic appearance of the WR fault, it is instructive to analyze the PC thrust; the two faults' geometry and mechanism appear to be similar. About 20 km to the SW of the WR thrust, the PC thrust may have been an embryonic WR thrust which did not develop fully. Clearly seen from 10-13 km depth, the PC thrust's reflections can be continued (with controversy) to 16 km depth on the enlarged sections. The seismic character of the two faults' reflections is ***remarkably*** similar (Figures 3.3, 3.14). The reflections are high-amplitude, three-legged (three cycles) events. The Precambrian crystalline basement juxtaposed by the PC thrust is ***not*** considered to have significantly different lithologies or seismic impedances. Therefore the reflection is interpreted to be from the PC ***fault zone***. Vertical offset of 600 m is observed in the lowermost GR basinal sediments. This movement, 1/50th

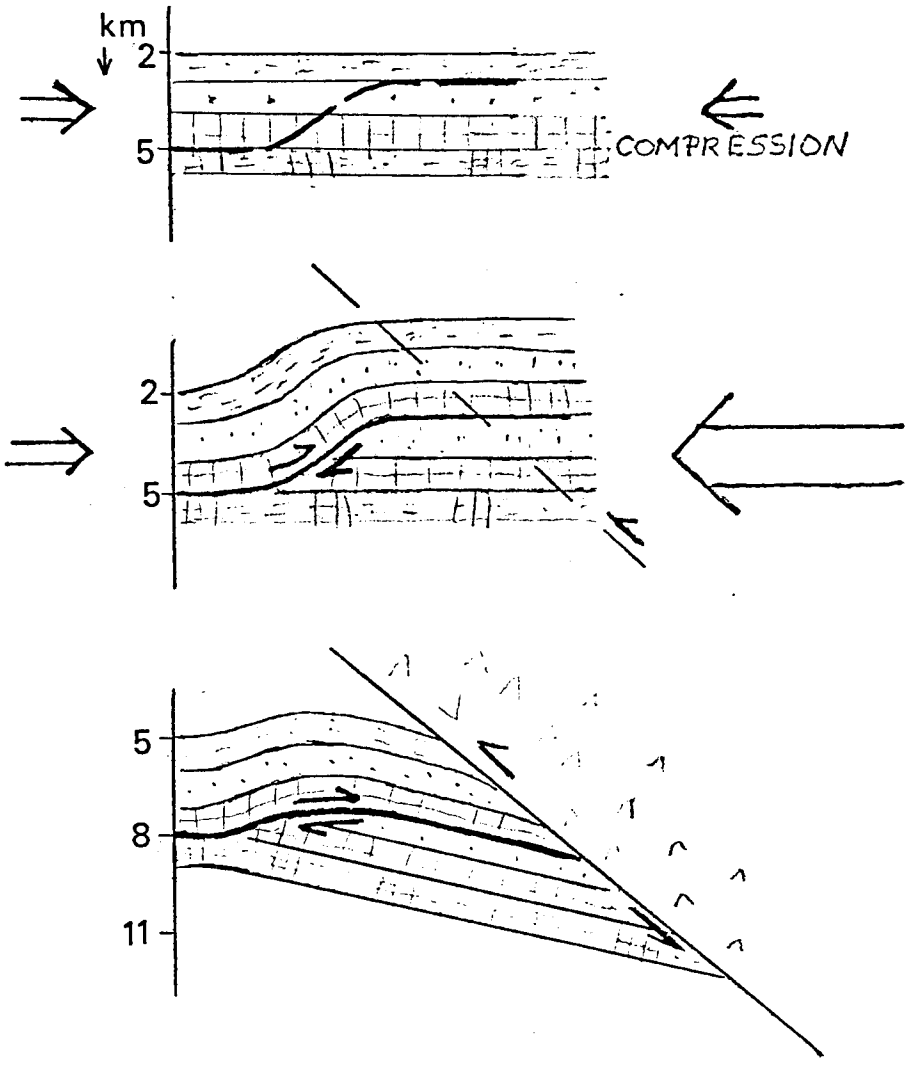

FIG. 3.29. Simplified conceptual sketch showing the doubling of the Madison and adjacent formations due to compression before (during?) WR thrusting.

the total displacement of the WR thrust, created the necessary conditions for a seismic reflection. Therefore, any splays or subordinate faults of the WR thrust with offsets on that order can also be expected to be seismically visible. Below 13 km, the reflected energy from the Pacific Creek thrust fault traveled through the complexly deformed surface rocks where the WR thrust subcrops. The complex near surface geology probably obstructed the coherent Pacific Creek thrust reflection and/or processing failed to enhance the reflections. Since even the GR sedimentary reflections did not appear clearly on the stacked section under the WR thrust (and we know that *they* are there), we attribute the poor quality PC thrust reflection below 13 km to the complex "near surface" geology and/or processing.

Smithson has suggested (pers. comm.) that the reflections interpreted to be from the PC thrust (C, Figure 3.3; B, Figure 3.14) may be sideswipe which just happens to migrate to its position under the PC anticline. This interpretation, while possible, is not preferred because: 1) the migration velocity at the depth of the reflection is ~6 km/s. If the reflection were sideswipe from an inhomogeneity in the sedimentary column, dramatic overmigration ("smiles") should be observed, and was not. If the reflection was sideswipe from within the basement, then a velocity of ~6 km/s would migrate the event with no apparent artifacts, which leads into the next point. 2) Geologically, we expect to see Laramide anticlines underlain by thrust faults. The fortuitous movement of sideswipe from a basement inhomogeneity into exactly the area where we are geologically expecting a reflection is considered unlikely. Moreover, we expect that further processing efforts may enhance the PC thrust reflection from 8-10 km depths (where we do not now see a reflection).

The overall apparent dip of the WR thrust is ~30 degrees to ~32 km depth. Figure 3.30 is our interpretation of the migrated data. Careful examination of the migrated data reveals that the reflections from the fault zone are uneven and segmented. With depth, each segment is tangent to a more steeply dipping line. An individual dip segment is concave upward such that the local appearance is one of "dip-flattening." This can be seen even on the unmigrated data. It is even

more obvious on the migrated data. Various strands of the WR thrust appear to splay out at 6.6, 18, and 25 km, and bottom at 32 km depth. The width of the fault zone thickens with depth.

Below ~13 km depth, the WR "fault zone" acquires many more diverse strands, such that an explosion of reflectors is observed (Figure 3.21). It is known that continental earthquake foci are not observed below ~15-20 km depth. Deformation there is thought to occur throughout a volume and not be necessarily confined to a "single" fault plane. This area of "volumetric deformation" is seismically observed to start on the WR data at ~13 km depth. What is now observed at ~13 km depth was deeper, perhaps at ~20 km depth, at the start of Laramide deformation.

About 50 km (horizontal extent) of the hanging wall block of the WR thrust appears to have been involved in the crustal shortening by low angle (~30 degree) thrust faulting (see Figures 3.21, 3.25, and 3.30). The style of deformation in the hanging wall as interpreted from the number and character of reflectors is different from that in the footwall. The hanging wall has many more reflections in it paralleling the WR thrust, suggesting splintering, subordinate splays, and volumetric deformation, along a myriad of slip zones. The (lower crustal) footwall adjacent to the WR fault has far fewer reflections and appears to have not undergone such extensive shattering.

We here interpret a decrease of offset with depth on the WR fault: 6-8 km vertical offset at 22 km depth compared to ~14 km vertical offset at the surface. The band of deep crustal reflections at 22-24 km on line 1A interpreted by Smithson *et al.*, (1979) as part of a recumbent fold, appears to continue at ~14 or ~16 km on the other side of the WR fault. This interpretation suggests a set of fault planes such that some segments or splays do not reach the lower horizons, or a flattening of the major fault plane such that with increasing depth horizontal movement predominates over vertical movement.

The general style of Laramide deformation has been described as a two-step process: folding to generate an asymmetric anticline and then faulting of the oversteepened limb. Any interpretation of the WR thrust

FIG. 3.30. Structural interpretation of the Wind River COCORP migrated data. The WR thrust (right) and the Pacific Creek thrust (left) are shown. The WR thrust fault is seen to ~32 km depth, at an average dip of 30 degrees. It is composed of several strands in a complex wide zone of deformation, extending at least 50 km laterally. Fault reflection dip segments flatten at 6.6, 12, 18, 25, and 32 km depth; these can be interpreted as thrust splays or as local slip zones. The flattening of the fault zone with depth tilts the WR basin sediments, and permits less vertical offset at depth than at the surface. Zone A' is interpreted as offset 6-8 km by the WR thrust from zone A.

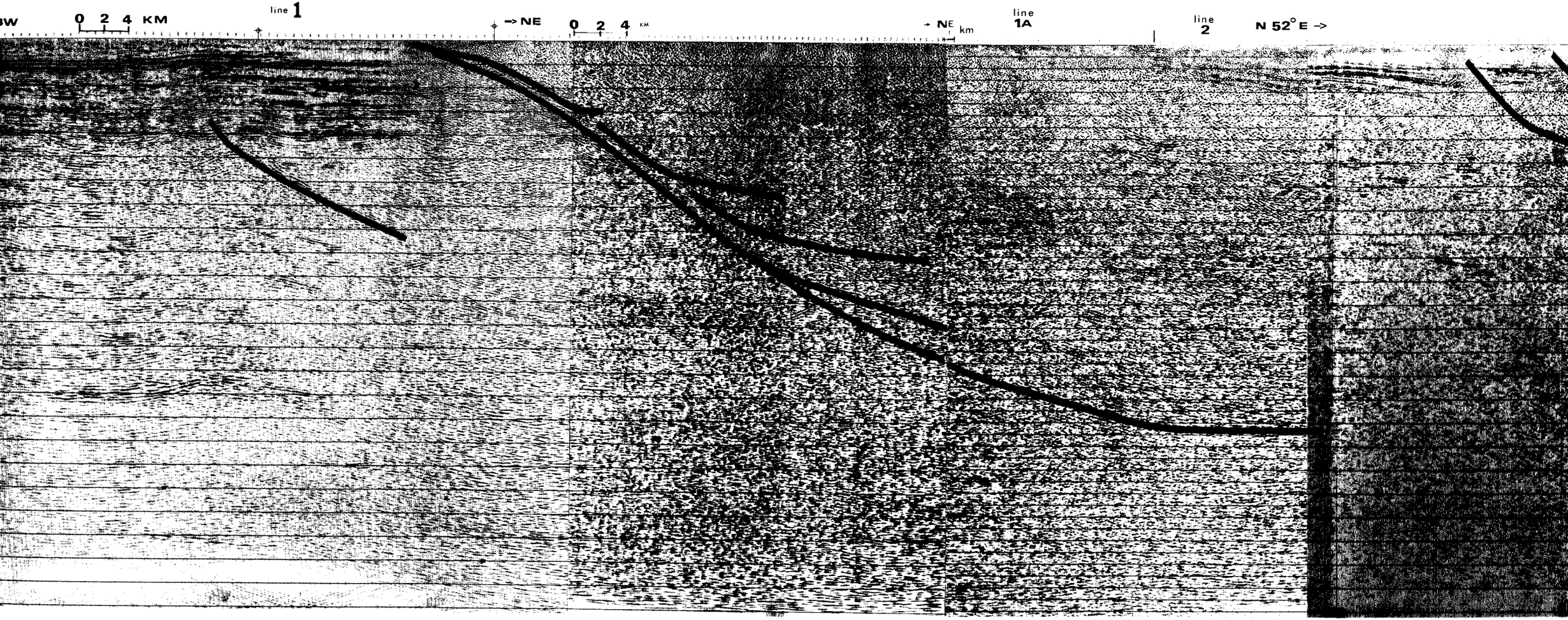
SW
0 2 4 KM
line 1
→ NE
0 2 4 KM
→ NE km
line 1A
line 2
N 52° E →

with respect to Laramide deformation should consider the following constraints: the minimum vertical and horizontal offset required by projection of the Cambrian-Precambrian contact, the geologic evidence of folding in the WR Range associated with the faulting, the failure to see Moho offset in the gravity data although offset of intermediate-depth crustal boundaries is consistent with gravity models (Smithson *et al.*, 1979), the observed tilt of the WR Range and basin sediments, and the decrease of offset with depth as suggested by the migrated data. Our alternative explanation to the general "fold then fault" description of Laramide deformation is one wherein faulting, folding, and tilting occurred contemporaneously. (The folding is exhibited by the tilt of the sedimentary rocks on the east flank of the WR Range.) The geologic map of Wyoming (Love *et al.*, 1955) shows sedimentary rocks curved around the northern end of the WR Range, and to a lesser extent around the Range's southern end (Figure 3.1). This geologic evidence is consistent with but does not prove folding prior to faulting in the WR thrust area. In the Pacific Creek thrust area, the seismic data indicates that folding in the uppermost sediments was the response to faulting in the basement; one accompanied the other. Simplified conceptual models, scaled from the migrated data, were made to study alternative interpretations of the WR fault. The paper models illustrate the tilt of the WR sediments as related to movement along an arcuate WR fault plane.

We used the simple geometric relationship

$$\text{tan of dip, WR seds.} = \frac{\text{Length of displacement along arc}}{\text{Radius of fault curvature}}$$

One model produced 7 degrees of tilt in the (originally horizontal) WR basin sediments by inducing 27 km of slip along an arcuate fault plane tangent to a 30-degree dipping plane at the present earth surface. The radius of the (circular) arc was 219 km. The fault on the model extended to 28 km depth. The lower crust presumably deforms more nearly plastically (or volumetrically) and thickens. The migrated data shows ~ 7 degrees of tilt for the WR basin sediments.

Our preferred model (Figure 3.31) produced 12 degrees tilt in the WR basin sediments by 26 km total slip along the WR fault. The total

slip is modeled as the sum of displacements along arcuate fault planes and linear fault planes. In the model, the conceptual arcuate fault plane flattened at 27 km depth; the radius of the arc was 122 km. The conceptual linear fault plane extended to 30 km depth. Vertical offset of 13.3 km at the surface, and 10 km offset at 20 km depth, was produced. While this conceptual model is not intended to match the observed data exactly, it reproduces observed fault curvature, tilting, and a distinct, more nearly planar lower boundary to the fault zone.

DISCUSSION

The data allow somewhat more speculative interpretations. The interpretation and the significance of the large-scale (> 5 km x 5 km) and small-scale (< 1 km x 1 km) seismic features, while controversial, are presented here. The seismic data offer new insights into the effects of large-scale faulting. The effects of such faulting can be divided into upper crust (0-~15 km depth) and lower crust (~15-40 km depth), and further subdivided into hanging wall and footwall. Different phenomena in footwall vs. hanging wall in the upper crust are seen in outcrop and subsurface data, and can be interpreted in the migrated data.

Fault Zone Mechanism: Deformation in the Fault Zone and Hanging Wall

The reflections from the upper crustal WR fault zone can provide significant insights into the mechanism and mode of deformation when properly imaged. The migration of the initial stacked sections can give hints as to structure and mechanisms; reprocessed stacks and their migrations can be used to test the following interpretations.

Any proposed fault zone mechanism should explain the dip segments which flatten with depth. Of the many possible explanations, we favor the following two. (1) Irregularities in the fault zone have been sheared off during thrusting and have remained trapped in the fault zone. First movements may have been irregular, and later movement would

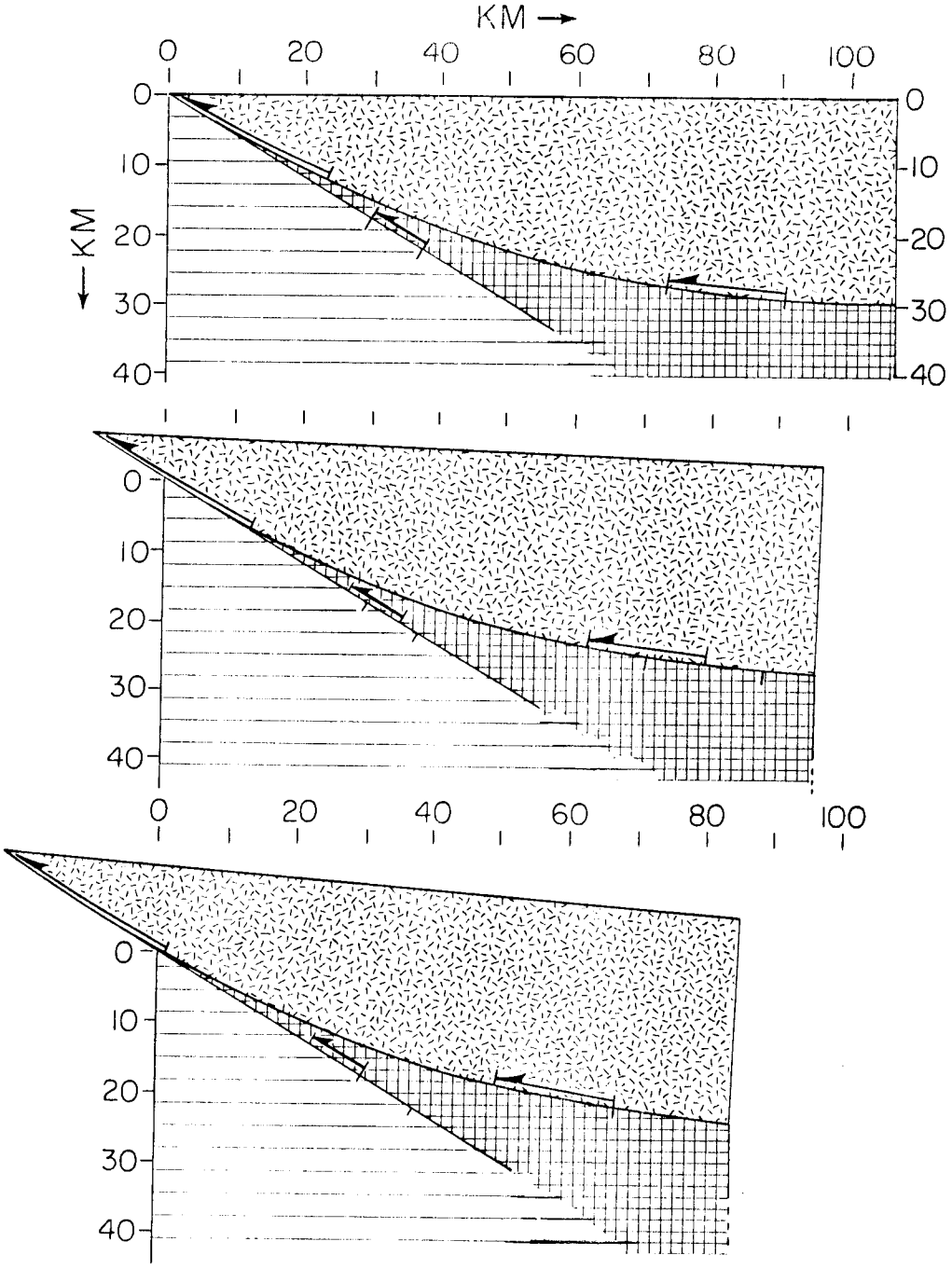

FIG. 3.31. ***Conceptual*** model of the WR thrust in action. Upper diagram: before faulting; middle diagram: partial offset; lower diagram: after Laramide displacement. Top of diagram represents top of Precambrian. The total displacement along the WR fault zone (long arrow, upper left, each figure) is the sum of the displacements along linear parts of the fault zone (short arrow, middle of figure) and curved parts of the fault zone (arrow, lower right). The constraints used to generate this ***simplified*** model were the minimum vertical and horizontal offset seen at the surface, the geologic evidence of folding (or tilting) associated with the faulting, the failure to see Moho offset in the gravity data although offset of intermediate depth crustal boundaries is consistent with the gravity data, the observed tilt of the WR basin sediments, and the decrease of offset with depth as interpreted from the migrated data. This model produced 12 degrees tilt in the WR basin sediments by 26 km total slip, partly along an arcuate fault plane (122 km radius) flattening at ~27 km depth, and partly along a linear fault plane (to 30 km depth). The model displays vertical offset of 13.3 km at the surface and 10 km offset at 20 km depth.

have made a smoother fault plane, as suggested by Smithson *et al.* (1979). These fragments of Precambrian rock appear seismically as lenses ~1x2 km in dimension. Although brittle deformation has occurred, the overall effect resembles ductile deformation because these fragments in the fault zone are cut out of zones of compression/overlap and (can) move preferentially towards the "empty" or "gap" zones. This suggested mechanism also takes care of the space problem, for these fragments are sheared off of zones of overlap and fill the zones of gap. An outcrop analogue on a very much smaller scale is seen in Figure 3.32. In the seismic data, we do not as readily observe the tops to these lenses as the bottoms.

(2) The alternative, or complementary, explanation is that increasing deformation is seen in the upper crustal hanging block as the fault zone is approached. The hanging wall appears seismically to be broken up (more reflectors); the footwall appears seismically to have suffered comparatively less deformation (less reflectors). Note the significant fault reflections NE of the major WR fault reflections in Figure 3.17 (D). This preferential fracturing (***and/or*** offset, in the WR thrust case) in the upper block is a common observation in mining geology, and was described by Thompson (1966) in the driving of the San Jacinto tunnel, California. The tunnel was cut in massive Cretaceous granitic rock (granodiorite, quartz monzonite, and quartz diorite) and older metamorphic rocks (Paleozoic? - mica schists, quartzites, and crystalline limestones) through part of the San Jacinto fault system. The tunnel lies in the 30 km between the San Jacinto fault zone and the San Andreas just south of the San Bernadino Mtn. Range near Banning, Ca. The two adjacent major fault zones are strike slip; the smaller fault systems between the larger fault zones in this region usually have an oblique-thrust sense of displacement. The following observations in the tunnel were made in rock currently 300 m below the surface. The depth at which faulting took place is unknown.

> [In the hanging wall] as the heading neared the fault **the open fractures were more numerous and the volume of inflow [of water]** ***increased***. Normally by the time the footwall was reached, **where gouge and crushed material was present,** the

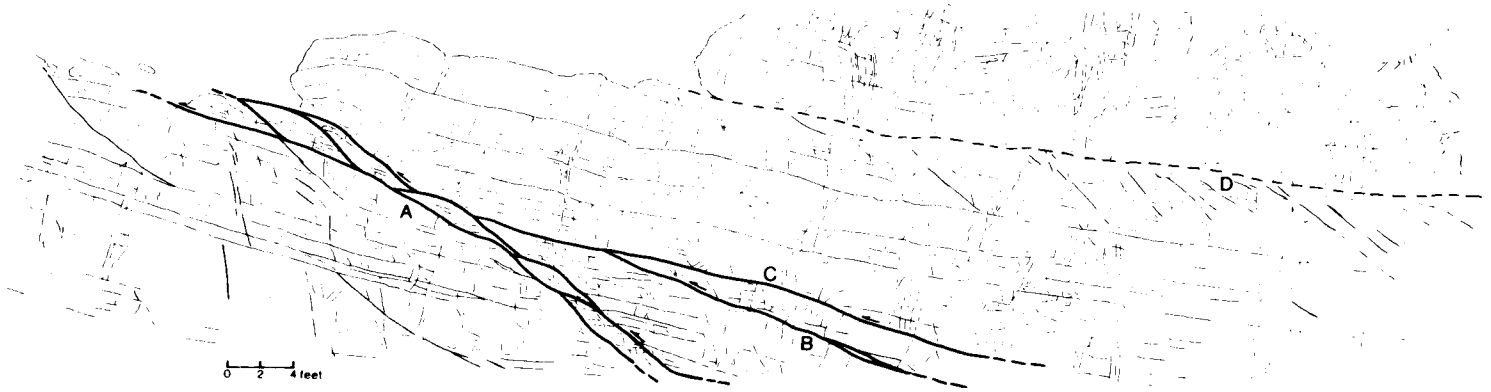

FIG. 3.32. Picture of outcrop showing conceptual analogue on a much smaller scale for the 1km x 1 km chips seen seismically in the fault zone.

> hydrostatic head had generally been reduced to the extent that little difficulty was encountered in driving through **the soft, faulted material characteristic of the actual planes of slippage.** Conversely when the headings were being advanced ...through [the] **footwalls,** large flows of water under very high pressures were freed **instantaneously** [upon penetration of the plane of slippage], resulting in strong surges that carried large quantities of broken rock, sand, and clay gouge into the tunnel (Thompson, 1966). [Emphasis, this paper.]

"Open fractures at the footwall are few, and the gouge and crushed material present an almost impermeable diaphragm to the waters which may percolate more or less freely along the open fractured hanging wall" (Henderson, describing the San Jacinto tunnel, 1939). Peak flow was measured at 40,000 gal/min, and some 3000 cubic yards of "sand" (thought to be fault rubble) poured into the tunnel along with the water, considerably slowing progress. In the Green River Basin, on line 1, station 301, the presence of water and porosity at 20,000 ft was demonstrated by 6425 feet net rise of water, muddy water, and gas-cut mud in the Superior Pacific Creek Unit 1 from the Upper Cretaceous Frontier Fm (19765-20521 ft).

Either large-scale fluid-filled fractures, *i.e.*, macro-fractures, or offset, can cause reflections in the upper portion of the fault zone: fluid in the fractures could make ***that*** region of rock different in seismic impedance than the adjacent "tight" unfractured granite, and thus reflective. The fractures which are observed to exist in and around fault zones will lower the density and the velocity, which will thereupon cause a seismic impedance contrast. Offset as a possible cause for reflections is treated in the next section. The application of Thompson's (1966) and Henderson's (1939) observations to the WR area would be as follows: the scale of fracturing/offset goes from cms to meters to hundreds of meters to kilometers as the fault zone is approached in the hanging wall. The ***start*** of fracturing/offset (the upper limit of the "fault zone") in the hanging wall is seismically transparent; the scale of deformation gradually becomes that detectable by seismic methods (3/8ths of a wavelength, or ~100-200 m). The bottom

of the fault zone where the concentration of slippage planes may exist, is seismically reflective. The bottoms of the major slip boundaries, as seen seismically, are ~2-4 km in length, curved, dipping ~30 degrees at the top, and decreasing in dip with depth to about 5 degrees.

Cause of the WR Thrust Reflection

The argument as to ***why*** the fault zone is seismically reflective will probably continue for years. The obvious four possibilities are: (1) water-filled fractures or pore space within the fault zone (or relatedly, water, trapped under pressure, in the fault zone). (2) The juxtaposed blocks have ***different*** seismic impedances; the fault zone width is negligible, seismically, or the seismic impedance of the (wide) fault zone is like that of one of the blocks, such that the fault reflection is basically attributed to the juxtaposition of block A to block B. (3) The fault zone constituents (gouge or mylonite) have different impedance properties than the upper and lower blocks. Unfortunately, the velocities and densities of mylonite and gouge are not in the literature, which prevents an estimation of reflection coefficients at this point. The seismic impedance contrast may be due in part to anisotropy, or to a different Q. (4) A variation of (3) is different mineralogy within the fault zone, caused for example by hydrothermal alteration or deposition, or shear deformation causing a layered redistribution of elements. The Pacific Creek fault juxtaposes "identical" Precambrian rocks with only 0.6 km offset and creates a substantial reflection. Therefore either (3) or (4) or both would appear to be valid there. In the upper parts of the WR fault (~first 5 km), the fault zone is seismically visible and at least 1 km thick. The American Quasar well data shows this clearly. The mud log records granite with traces of chlorite from 0-2.04 km; "granite wash, poorly sorted," from 2.04-3.08 km, which is to be interpreted as "granite fault-breccia"; and sediments below 3.08 km. The TD was 4.585 km. The migrated data (Figure 3.10) show the highest-amplitude WR fault reflection at the top of the "granite wash" zone, NE dipping reflectors from 2-3 km, and again a good reflector at 3 km at the base of the "granite wash." The migrated data, although AGC'd, suggest that at this location in the Wind River

Mtns. the greater impedance contrast is between the granite and the "granite wash," than between the "granite wash" and the sediments at 2-3 km depth. In the upper parts of the WR fault, (1) may explain the WR fault reflection.

To approximately 10 km, hypotheses (1) and (3) may be the reasons for the fault reflection. In the middle crust (10-20 km depth), porosity may be zero due to pressure and temperature, so (1) might not be valid. If mylonite constitutes the zone of slippage in the lower parts of the WR thrust, and it has significant anisotropy, then (3) or (4) may be the preferred explanation.

Migration artifacts can give clues as to velocity distributions in the earth, and hopefully in the area of the WR thrust zone. When the same velocity was used to migrate the thrust zone as the neighboring rock (6.1 km/s), some overmigration apparently resulted on the 1A line (2-16 km depth, Figure 3.21). No migration artifacts appeared when the upper crustal data was migrated at 4.5 km/s (Figure 3.22). This may indicate that the thrust zone is of a slower velocity than adjacent rocks. Alternatively, the overmigration "smiles" may simply be indicating that the overlying media (the hanging wall) has been assigned too high a velocity, or that the "line straightening" process induces artifacts on the migrated sections. Determining crustal velocities by analyzing a series of depth migrations (using the best stack possible), and choosing the best imaged dataset as a possible solution of the earth structure, is a powerful tool for studying the crust.

Detailed analysis of the stacking velocity functions of line 1A will shed light on the nature of the WR thrust reflections. Essentially one stacking velocity function was used to stack in about the first two-thirds of line 1A (the part without Wind River Basin sediments) even though high-amplitude reflections with significant dip are present. The presence of dip (in sedimentary sequences) nearly always indicates lateral velocity variation. Here, dips are present, with little variation in the stacking velocity. (Perhaps future reprocessing will indicate lateral velocity variation, especially slower velocities in the fractured hanging wall.) The lack of variation in the initial stacking

velocity functions suggests that the WR fault may be juxtaposing crystalline rocks of the same velocity/density. This hypothesis would thereupon suggest that the WR fault reflections are caused by the seismic impedance contrast in the constituents of the fault zone (mylonite? gouge? vein material? rubble filled with trapped, over-pressured water?). The average stacking velocity function for the 1A line is given by (time in sec, velocity in km/s): (0, 3.05) (0.1, 3.96) (2.4, 4.57) (3.5, 5.18) (5., 5.79) (8.25, 6.4) (20., 7.0).

The degree of fracturing of the granite may also be determined by a detailed velocity analysis on line 1A: if interval velocities really *are* approx. 4.5 km/s in the upper 5 km of the entire hanging wall (approx. 23 km of lateral extent of exposed Precambrian), then widespread fracturing is indicated. (Usually only the leading edge or toe of thrusted Precambrian would be expected to have such low velocities.)

The two bands of energy within the Precambrian upper crust under the WR basin sediments on line 1A (C, D, Figure 3.21) may be low-angle (15-degree) thrust faults. If the trend of the lower band of reflectors is projected to the surface, through the dip segments at 2.5 km, the (postulated) thrust appears at the northeastern edge of the Tertiary fill. Figure 3.33 shows a scenario wherein a wedge of post-thrust fill may accumulate in front of a thrust. An alternative interpretation is that the reflectors represent gabbro layers or layered pyroxene granulite within granite gneiss (Smithson *et al.*, 1979). These possible thrust faults provide a possible explanation for the low interval velocities of 4.5 km/s which are indicated by the initial processing.

The thrust faults offsetting the WR basinal sediments may have similar geometry, but are on a smaller scale. Speculatively, they may root in the upper crustal band of reflectors at B, Figure 3.28. The base of the sedimentary section in the Sand Draw anticline (center of line 2) has 1.3 km offset. There appears to be ~1 km offset on the adjacent thrust fault (to the NE). The data do not show clearcut fault reflections here, although faint, steep, NE-dipping shallow crustal energy (4-10 km depth) can speculatively be attributed to the thrust faults.

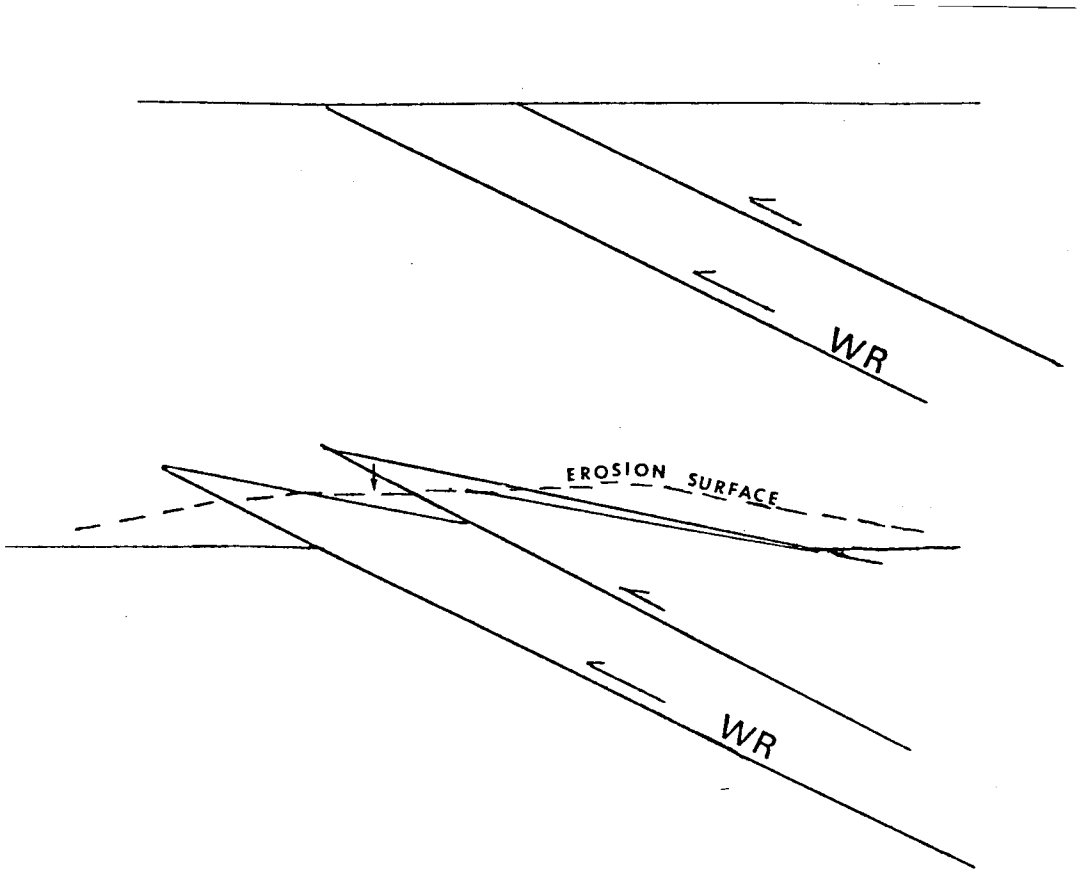

FIG. 3.33. Sketch showing the accumulation of a depositional wedge of fill in front of a thrust. Deposition is thought to occur during and after thrusting.

High stacking velocities should be examined in this region to see if steeply dipping crystalline reflectors may be brought out and then migrated. Sub-optimum processing, and the drop in seismic coverage (fold) due to both the nearby producing fields and the end of the line probably cause the poorer quality data here.

Amplitude Variations along the WR Thrust Reflection

The amplitude of the fault zone reflections (top and bottom) varies with depth: sometimes the top appears more reflective (2-3 km depth, Figure 3.20, B and C) and sometimes the bottom (10 km depth, B, Figure 3.17; 20-22 km depth, A, Figure 3.22). Part of this effect might be caused by processing; incorrect stacking procedure (in this complicated region) will degrade the quality of the reflection. If sophisticated reprocessing confirms the general results from initial processing, namely that the amplitudes do vary, with the bottom of the fault zone often being the higher amplitude reflection, then the following discussion may help explain the observation.

To postulate different reflection coefficients for the top and bottom of the fault zone is to postulate different physical contrasts at the top and bottom of the fault zone. Weber ***et al.*** (1978) concluded that there exists a zone of porosity increase in the hanging wall and a porosity decrease in the footwall of normal fault systems in sandstones. Thompson's work (1966) also showed differences between the hanging wall and the footwall in and near faults. The model proposed is a footwall block which is comparatively unfractured, a fault zone wherein the slip "plane" (a zone of dislocation thick enough to be seen seismically) tends to be on one side or the other, and a hanging wall with a myriad (network) of faults (or fluid-filled fractures) which increase in number and thickness as the fault zone is approached. Seismically, this situation would produce: a footwall block with reflections only from lithologic contrasts; a higher amplitude reflection from the side of the fault zone where the slip plane is; and a hanging wall with many reflectors which decrease in number with distance away from the fault zone.

Effect of the WR Thrust on the Footwall Sedimentary Section

Seismic interpreters working in the thrust belt use certain basic techniques (Sacrisson, 1978). A few of the standard concepts are: (1) faults cut up section in direction of tectonic transport; (2) faults are parallel to bedding within incompetent rocks and are oblique to bedding within competent rocks (see Figures 3.18, 3.34); (3) thrusts are known

(recognized) by the interruption of stratigraphic sequence (layered reflectors); and (4) normal (extensional) faulting in Wyo., Utah, and Idaho, generally took place after the major thrust faulting. The majority of such faults are restricted to the thrust's hanging wall (Royce, 1975).

The disappearance of the WR thrust reflection from 7-9 km depth, if caused by geology and not processing, may signify a change in the style of deformation. As the thrust leaves Precambrian crystalline basement at ~10 km (competent rocks), and enters the sedimentary layered (weaker) rocks, subsidiary faults may splay into the sedimentary sequence parallel to bedding. This idea, shown in Figure 3.34 from 5-10 km depth, can also be interpreted in Figure 3.17. In the Green River Basin north of the COCORP line, Sacrisson (1978) used this concept of deformation to interpret his reflection data (Figure 3.35).

The contrasts in rock properties (anisotropy and strength) can explain why subsidiary thrust splays are developed in the footwall sedimentary sequence. Interpretation here is further complicated by the postulated thrusting along southwesterly dipping planes which produced a repeated Madison limestone section prior (concurrent?) to WR thrusting, as discussed earlier (Figure 3.29).

In the unmigrated data (Figure 3.4), the change in dip of the thrust at 10 km depth is indicated between 3.0-3.5 sec. However, this observation required substantiation on a migrated section to confirm the hypothesis.

Thickness of WR Thrust

The thickness of the Wind River thrust zone as a function of depth may be estimated from the migrated data (Figures 3.18, 3.21). The fault zone is covered by upper Eocene rocks (Bridger Fm.) at the surface. Reflections from within the Tertiary wedge to a depth of 1.5 km obscure the fault zone's true thickness. At 2.0 km depth, the fault zone is 1 km thick (known from well data). The migrated section (B, C, Figure

3.20) also shows a fault zone 1 km thick at the well. The fault zone there is slightly lower in velocity than the unfractured granite. An increase in dip angle coincides with an apparent "thinning" of the fault zone to 500 m at 3 km depth. By 4 km depth, the fault zone is 1 km thick. The seismic expression of the thrust zone widens with depth after that, to reach an (apparent) thickness of 2.25 km at 5.5 km depth. Between 6.5 and 9.0 km depth there is a reflection "gap" from the main thrust. At ~9.5 km depth, energy dipping at 30 degrees is interpreted to be from the WR thrust; the thrust zone appears to be 2 km thick at that depth. At 6.5 and 12 km, fault splays or strands flatten with depth. At 16 km (Figure 3.30), the fault zone is at least 4 km thick; from 16-32 km the thrust zone has multiple strands. Each strand is ~500 m to 1 km thick.

Multiples

Short-period multiples, generated within the GR and WR basinal sections (lines 1 and 2), were attenuated by the adaptive deconvolution and filter before migration (Wallace, 1979). Depth sections distort the timing relationships of multiples, and so the migrated data presented in this paper are not useful for multiple identification. Smithson ***et al.*** (p. 5960, 1979) cited the ***general parallelism*** of deep reflections with surface structure in sedimentary rocks as one point of evidence for long-period multiple reflections contaminating the basement data. In the migrated sections shown here, line 1 shows dipping deep crustal reflectors ***and*** flat ones, such that general parallelism is not seen; line 2 with its dipping sedimentary reflectors exhibits both flat and slightly NE dipping reflectors. In general, parallelism in the character of the shallow and deep reflections does not conclusively prove that the deep events are multiples. If density stratification or thermal- or pressure-controlled metamorphic boundaries in the crystalline crust tended to make predominantly subhorizontal seismic reflectors, and if the whole upper crust to a depth of 32 km was later thrusted and tilted (as suggested in our model), then the once subhorizontal deep reflectors may have up to as much tilt as the sediments. The dip of the basement reflectors in the hanging wall of the WR thrust is generally less than

FIG. 3.34 (opposite). Speculative interpretation showing deformation in the sediments under the WR thrust.

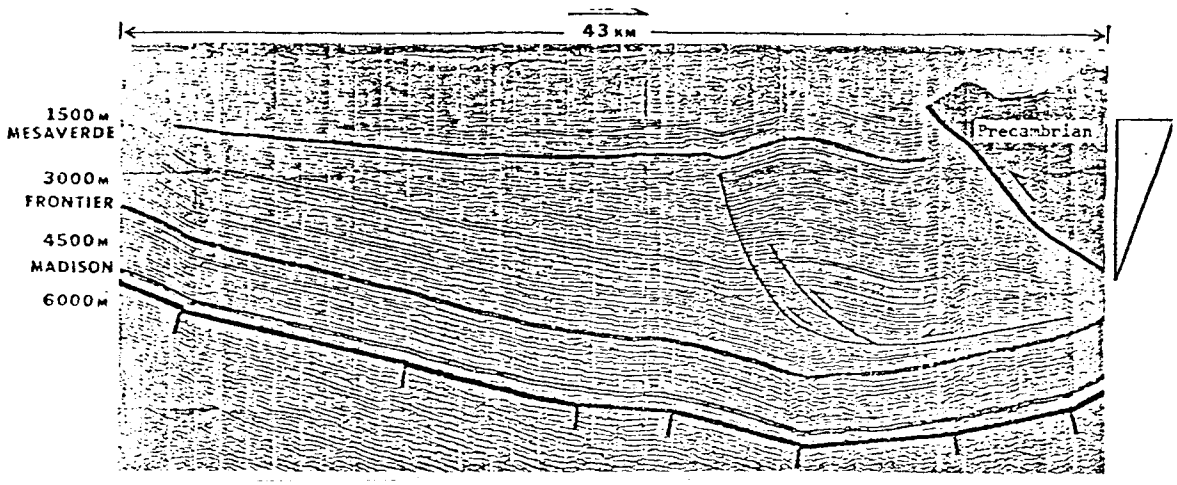

Seismic section, northern Green River Basin, Wyoming.

FIG. 3.35. Unmigrated time section from the northern Green River basin, north of the COCORP line, showing thrust splays into the sedimentary section. The shaded area in the upper right is a Precambrian "basement block that has emerged at a low angle (~20 degrees). The sedimentary layers to the left of the basement block have been end-loaded" (from Sacrisson, 1978).

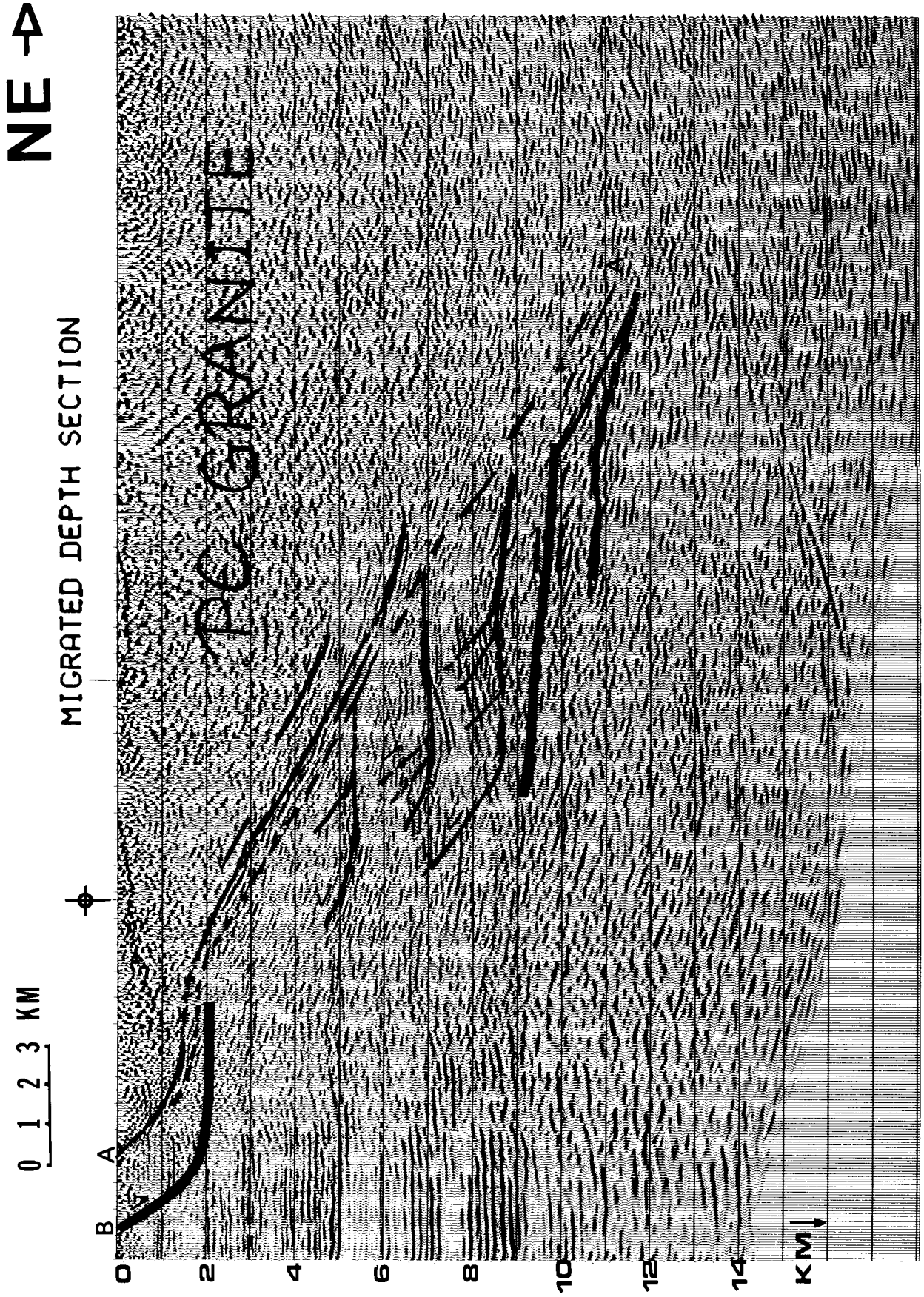

FIG. 3.34.

the dip observed in the WR basinal sediments, which suggests that there were thrusts in the hanging wall which also flattened with depth. The intermediate and deep crust appears to have been tilted less than the upper crust.

The ***different*** appearance of the crystalline crust on line 1A where no sedimentary layers were present was another argument cited by Smithson ***et al.*** (p. 5961, 1979) for rejecting the deep events on the 1 and 2 lines: where little or no sedimentary-generated multiple energy would be expected, crystalline "reflections are much less common, and weaker, and with divergent dips and less regular character." After migration, the crystalline crust on line 1A has a ***similar*** appearance to that of the deconvolved 1 and 2 lines as on the 1A line. Bands or zones of reflectors are seen on lines 1, 1A, and 2.

An interesting facet of crystalline seismic reflection interpretation is the processing and interpretation of periodicities (up to ~0.300 sec), where ***no*** sedimentary layers overlie basement. Line 1A may contain a significant amount of energy with periodicities up to ~.3 sec (pers. comm., Mark Bronston). The conventional interpretation of "interbed multiples" may not be correct here: the periodicities may be the valid band-limited seismic response to the foliated or gneissic crystalline rocks, and as such, constitute signal and not noise. Mayer (1979) and others have described the significant effect that "tuning" or interference between many layers of small reflection coefficients has on band-limited data. Universal direct correlation of one reflection to one geologic horizon is not found or expected in reflection seismology. Reflections are known often to be the composite response from many small layers.

The WR fault is interpreted to extend to at least 25 km depth, and probably to 32 km depth, because we picked the marked reflections (Figure 3.30) as primary reflections from the WR fault. If later work proves that these reflections (from 26-32 km depth) are not geologically generated or are multiples, then our interpretation must be revised to honor only primary reflections.

CONCLUSIONS

Depth migration with the thin lens term provides geophysicists with a powerful tool to image the crust even in areas of severe lateral velocity variation. The migrated COCORP WR data show the WR thrust extending to 32 km depth with an apparent dip of ~30 degrees. It is composed of many strands in a complex wide zone of deformation affecting ~50 km (laterally) of the crust. Subsidiary strands splay out at ~12, 18, and 25 km depth. The reflections at these depths, at or below the base of continental earthquake foci, may indicate that deformation in the intermediate and lower crust takes place over a large volume rather than a discrete fault plane/zone. Offset of 600 m along the Pacific Creek thrust produced a high-amplitude fault reflection which initial processing enhanced at 10-13 km depth. Offsets on that order (and presumably larger) can create a fault zone such that seismic reflections result even though "identical" crystalline basement rocks are juxtaposed. The geologically known displacement along the WR thrust, the interpreted decrease in offset with depth (14 km vertical offset at the surface, 6-8 km at 22 km depth), the tilt of the WR basinal sediments, and the lack of Moho offset (inferred from gravity data) can be explained by a simplified conceptual model showing in cross section 26 km of WR fault displacement; in the model, the net displacement is the sum of offsets along linear slip planes and arcuate slip planes (Figure 3.32).

Several smaller scale features have been somewhat more speculatively discussed. The WR thrust had different effects on the footwall (sedimentary vs. Precambrian section) than on the hanging wall. The crystalline hanging wall (6-32 km depth) contains more reflectors than the Precambrian footwall, a fact which is interpreted to indicate that substantially more fracturing and deformation has occurred in the hanging wall. It is well known in mining geology that the hanging wall generally contains the fractures wherein the ore minerals accumulate. Two possible fault zone mechanisms as interpreted from the data are: lensoidal chips (~1 km x 1 km) sheared off during deformation become trapped in the fault zone and provide the asymmetric "ball-bearings" over which the thrust block rides. An alternative view of the data is that in the

hanging wall as the fault zone is approached, the scale of deformation increases from meters to 100s of meters. This was seen in the driving of the San Jacinto tunnel (through Cretaceous granite), California. The crystalline section of the footwall is relatively unfractured and undeformed. The thrust reflections may be due to a different seismic impedance in the constituents of the fault zone, as seen in the Pacific Creek thrust. The alternative migrations included show different details but support the major conclusions.

ACKNOWLEDGMENTS

This work would not have been possible without Jon F. Claerbout and all the Stanford Exploration Project members who provided the development and improvement of programs, the expensive computer hardware, and unlimited computer time to run the production-type jobs. Einar Kjartannson wrote and debugged the invaluable depth migration program. Rick Ottolini wrote the project program, and many other data-manipulation and processing programs, which greatly helped the whole COCORP Stanford project. Walter Lynn kindly wrote the program to display the velocity models used in migration. Don Seeburger and Russell Dyer provided many hours of good discussion and research work. Laura Gagnon helped run many of the migrations and organized the results; Rex Hanson spent many days and nights manipulating data on the computer, and deciphering the results. Research was funded by National Science Foundation Grant EAR 78-22762.

REFERENCES

Bayley, R.W., Proctor, P.D., and Condie, K.C., 1973, Geology of the South Pass area, Fremont County, Wyo.: U.S.G.S. Prof. Ppr. 793, 39 p.

Blackstone, D.L., 1963, Development of geologic structure in Central Rocky Mtns.: Backbone of the Americas: AAPG Memoir, v. 2, p. 160-179.

Braile, L.W., Smith, R.B., Keller, G.R., Welch, R.M., and Mayer, R.P., 1974, Crustal structure across the Wasatch Front from detailed seismic refraction studies: Jour. Geophy. Res., v. 79, p. 2669-2677.

Claerbout, J.F., 1976, Fundamentals of geophysical data processing: New York, McGraw-Hill.

Hayes, G.K., 1977, Analysis and interpretation of COCORP line 1, Wind River uplift, Wyo.: M.S. thesis (No. GEO610S), Geophysics Dept., Univ. of Houston.

Henderson, L.H., 1939, Detailed geological mapping and fault studies of the San Jacinto Tunnel line and vicinity: Jour. Geol., v. 47, p. 314-

324.
Jenkins, C.E., 1955, The Pacific Creek deep test, Superior Oil Co. No. 1 unit, section 27, T. 27 N., R. 103 W., Sublette, Wyo.: Wyo. Geol. Ass. 10th Annual Field Conf., Green River Basin, p. 153-154.
Kanter, L.R., Dyer, J.R., and Dohmen, T., 1979, in press, Laramide crustal shortening in the northern Wyo. province.
Keefer, W.R., 1970, Structural geology of the Wind River Basin: U.S.G.S. Prof. Paper, 495-D, 35 p.
Kjartannson, E., in preparation, 1979, Modeling and migration with the monochromatic wave equation--variable velocity and attenuation.
Love, J.D., Weitz, J.L., and Hose, R.K., 1955, Geologic Map of Wyoming, 1:500,000: U.S.G.S., Dept. of the Interior.
Mayer, L., 1979, The origin of fine scale acoustic stratigraphy in deep sea carbonates: Jour. Geoph. Res., v. 84, p. 6177-6184.
Oliver, J., Dobrin, M., Kaufman, S., Meyer, R.P., and Phinney, R., 1976, Continuous seismic reflection profiling of the deep basement: Geol. Soc. Amer. Bull., v. 87, p. 1537-1546.
Quam, S., 1978, Interpretation of the Wind River thrust, Wyo., as seen on migrated data: 1978 Fall AGU convention (San Francisco, Ca.).
Royce, F., Warner, M.A., and Reese, D.L., 1975, Thrust belt structural geometry and related stratigraphic problems, Wyo.-Idaho-N. Utah: in Deep Drilling Frontiers of Cent. Rocky Mtns., Rocky Mtn. Assoc. Geol. Guidebk., p. 41-54.
Sacrisson, W.R., 1978, Seismic interpretation of basement block faults and associated deformation: Laramide folding associated with basement block faulting in the western U.S.: GSA Mem., v. 151, p. 39-50.
Smithson, S.B., and Ebens, R.J., 1971, Interpretation of data from a 3.05-km borehole in Precambrian crystalline rocks, WR Mtns., Wyo.: Jour. Geoph. Res., v. 76, p. 7079-7087.
Smithson, S.B., Brewer, J., Kaufman, S., Oliver, J., and Hurich, C., 1978, Nature of the Wind River thrust, Wyo., from COCORP deep reflection data and gravity data: Geol, v. 6, p. 648-652.
Smithson, S.B., Brewer, J., Kaufman, S., Oliver, J., and Hurich, C., 1979, Structure of the Laramide Wind River uplift, Wyo., from COCORP deep reflection data and from gravity data, Jour. Geophys. Res., v. 84, p. 5955-5972.
Thompson, T.F., 1966, San Jacinto tunnel: in Engineering Geol., So. Calif., Special Publ. of Los Angeles Section of Ass. Engin. Geologists, p. 105-107.
Wallace, M., 1979, in press, Deep basement reflections in Wind River Line 1, COCORP Wyo. data.
Weber, K.J., Mandel, G., Tilaar, W.F., Lehner, F., Precious, G., 1978, The role of faults in hydrocarbon migration and trapping in Nigerian growth fault structures: Proceedings of OTC Conferences, p. 2643-2653.